Development and Comparison of 3D Dynamic Models of Golf Clubhead-Ball Impacts

by

Adam Caldwell

A thesis
presented to the University of Waterloo
in fulfillment of the
thesis requirement for the degree of
Master of Applied Science
in
Systems Design Engineering

Waterloo, Ontario, Canada, 2023

Author's Declaration

I hereby declare that I am the sole author of this thesis. This is a true copy of the thesis, including any required final revisions, as accepted by my examiners.

I understand that my thesis may be made electronically available to the public.

Abstract

The scientific understanding and modeling of impacts has led to major advancements in golf equipment performance. The latest generation of drivers allow golfers to hit the ball farther compared to previous models. Simultaneously, new clubs are more forgiving, resulting in poor shots to land closer to the target. Impact models are an important tool as they allow for computer simulations and optimizations to inform design decisions. Several driver impact models have been published for this purpose. Impulse-momentum (IM) and other analytical contact models offer fast simulation times. While finite element (FE) models are used to design clubs, they were not considered here as they require orders of magnitude more compute time. Many existing impact models have no or limited experimental validation to support their conclusions. From a literature review, several impact models were considered to develop golf-specific impact models. A significant portion of this research was identifying model parameters and quantifying the accuracy of these models. This was achieved using experimental data consisting of driver and 7-iron shots by elite players. This allowed for the accuracy of these models to be compared against each other.

Three IM-based impact models were used to predict the initial ball conditions for driver and 7-iron shots. The first model was referred to as the standard IM model as it followed the general methodology in the literature. The second IM-based model adds a small amount of mass to the clubhead and moves the ball centre of gravity slightly downwards to improve accuracy. These adjustments are intended to compensate for neglecting the shaft and ball deformation. The third IM-based model replaces the pure rolling assumption to allow a prescribed amount of slip at the contact point. This was motivated from experiments in the literature. The standard and adjusted IM models have been used to predict driver impacts. However, no published IM-based models exist to predict iron shots.

Three continuous analytical models were also used to model golf impacts. The first model was a volumetric normal force contact model with a two-layer ball and velocity based friction model. This model captures the tangential force reversal observed in experimental studies and FE models. From a literature review, two other non-FE models were considered as they also predict this tangential force reversal. These models were extended to be suitable for modeling golf impacts. A damping parameter was added to the normal force equations to make the predicted collisions inelastic. These models were originally developed for 2D collisions against a rigid plate. Here they were extended to a 3D multibody dynamics model to predict the collision between a golf club and ball.

For modeling driver impacts, the adjusted IM-based model was the most accurate overall. Ball speed was the most accurate launch condition with a mean absolute error (MAE) of 1%. The MAE for vertical launch angle and backspin was less than 10%. However, the MAE for sidespin and horizontal launch angle (azimuth) was between 30%-50%. The relative error of these two launch conditions was considerably greater for all impact models considered. For modeling iron shots, the two-layer ball with a volumetric normal force model was the most accurate of the models considered. The MAE for ball speed was 2%. The remaining relative errors were similar to the driver model.

From separate experimental testing, it was shown that amateur golfers hit the ground before the ball on nearly one-third of iron shots hit off the ground. Soil mechanics models were applied to the clubhead to extend the iron impact model to predict this type of mishit. This new model with ground reaction forces was used to predict the behaviour of iron strikes for off-centre hits. This model shows that irons follow the same trends as a driver for off-centre shots. Including the ground model results in a greater distance loss and the shot being significantly offline compared to the no ground model. While no rigorous experimental validation was performed for the ground model, the decrease in ball speed is consistent with experimental observations in the literature. This new iron impact model allows for design optimizations, previously performed for drivers, to be completed with iron type clubs.

Acknowledgements

I would like to thank my supervisor, Professor John McPhee for this opportunity and his invaluable experience in this field of research.

I would like to acknowledge the University of Waterloo and the Canada Research Chair for providing funding for this research.

I would like the acknowledge PING Inc. for providing the experimental data to validate the models developed in chapter 3.

Finally, I would like to thank all the members of the Motion Research Group for their suggestions and support.

Table of Contents

List of Figures

List of Tables

Chapter 1

Introduction

As of 2021, the R&A (The Royal & Ancient Golf Club of St Andrews) estimates the total number of golfers to be 66.6 million people globally [1]. This is an increase of 5 million in the last 10 years. In Canada, the participation rate is estimated to be as high as 19% of the total population [2]. Canada is home to over 2400 golf courses ranking it third globally [2]. As of 2021 the U.S. golf industry is estimated to be worth $84 billion USD, which is a 22% increase from 2011 [3]. A large amount of this evaluation is related to the manufacturing of golf equipment. To be competitive in this field, companies spend millions of dollars on research and development to give their clubs an advantage.

Modern golf club design increasingly uses advanced simulations to evaluate and optimize new designs. The driver has seen the most design changes compared to other clubs. Over the last 30 years, the average driving distance among professional players has increased by more than 30 yards [4]. These gains are largely associated with the equipment, as they coincide with the major design innovations [5–7]. Innovations such, metal clubheads and the three piece golf ball resulted in significant distance gains at the professional level the same year the they were introduced. [6, 7]. Due to the performance advantage and marketing strategies of golf equipment companies, enough consumers purchase a new driver every few years to fuel this progress. The driver is easily the most expensive club; most new models from premium brands cost over $500 USD.

In the last decade, the successful innovations developed for drivers have trickled down to irons [7, 8]. Previously, irons were made from a single piece of steel. Now, irons have variable thickness clubfaces to improve ball speed, and perimeter weighting to lower

centre of gravity and increase moment of inertia. Like the latest drivers, these features are designed to improve forgiveness and result in shots travelling further.

1.1 Motivation and Goals

Modern golf club design increasingly relies on computer simulations to evaluate the performance of new designs. Like the automotive or aerospace industries, models can inform design decisions while reducing development time and cost. Several researchers have developed impact models for this purpose. These models have been used to optimize loft, clubface geometry, center of gravity position, and other properties. However, the majority of published golf research is for modeling the driver. Several different methods have been used to develop impact models to predict the outcome of a golf shot. Impulse-momentum (IM) and other analytical contact models offer fast simulation times. Finite element (FE) models require orders of magnitude more simulation time but give insights into stresses and deformations experienced by the materials. Many of these models make assumptions to simplify the system. Furthermore, most models lack experimental validation to support the design recommendations suggested.

This thesis seeks to build on existing impact models to predict club performance. Several different impact models are developed and compared against experimental data. Three impulse-momentum models and three continuous contact models are considered. These models are used to predict both driver and 7-iron shots. The accuracy of these models is evaluated by comparing the models' predicted launch conditions to recorded shot data. Some driver impact models have been validated with experimental data. However, no iron models to date are three-dimensional or have been validated with experimental data. An iron model with similar accuracy to a driver model would allow for virtual experiments and club optimizations similar to driver models. Overall, constructing these impact models will build on the scientific knowledge of modeling and predicting golf equipment performance.

1.2 Contributions

- Developed and validated a parameterized golf iron impact model. This model predicts the initial launch conditions of a golf shot given the clubhead kinematics at the moment of impact.
- Extension of Cross and Dewhurst's 2D IM-based model to predict 3D impacts between a clubhead and ball. This model allows a prescribed amount of slip at the contact point and is used to predict both driver and 7-iron impacts.
- Modified existing 2D impact models (Maw and Arakawa *et al*) to predict inelastic collisions. These 2D impact models were extended to 3D models to predict impacts between a clubhead and golf ball.
- Applied soil mechanics models to predict the ground reaction forces when an iron impacts the ground. These forces are used in a dynamic simulation to predict the resulting launch conditions of the ball.
- A quantitative comparison of mishit behavior for a 7-iron. The effect of impact location on the clubface is analysed.

1.3 Document Structure

This Thesis is divided into five chapters:

- Chapter 1 gives a brief introduction and motivation behind this research. Here, the main contributions of this work are outlined.
- Chapter 2 provides background information about the game of golf and the evolution of golf equipment. This is followed by a literature review of existing impact models with a focus on modeling golf impacts. Finally, a short review of soil mechanics and terrain modeling methods is presented.
- Chapter 3 constructs several new golf impact models based on existing contact models. Six different impact models are considered. These are used to predict driver and

7-iron impacts with a teed ball. The accuracy of these models is evaluated using experimental data.

- Chapter 4 applies soil mechanics to predict the ground reaction forces when a club makes contact with the ground. This extends the impact model to predict shots hit off the ground, rather than just from a tee.
- Chapter 5 contains a project summary and outlines the work completed. From the results, recommendations for modeling impacts and future research are outlined.

Chapter 2

Background and Literature Review

Golf is a sport in which players use a set of clubs to make a series of swings to hit a ball into a hole. A typical golf course consists of 18 holes and the objective is to complete the course while making as few strokes as possible. In 1981, the average strokes per round was 72.33 on the PGA Tour [4]. In 2021, the PGA tour average was 71.27 strokes per round [4]. During this time, courses have steadily been getting longer. In 1981 Augusta National was 6905 yards from the tournament tees. In 2021, it was playing 7475 yards. Therefore, today's elite players are scoring lower on more challenging courses. Professional golfers have improved at every facet of the game in the last 40 years. The average driving distance has increased and putts per round have decreased. Like other sports, a component of this is due to the increased size and athleticism of golfers [9]. However, equipment advancements have played a major role as well [6]. This is demonstrated by many senior professional golfers, who are in their 50s, hitting the ball further compared to their 30 year old selves [5]. This chapter covers the basics of golf equipment, the history of impact modeling, and modeling methods for ground vehicles.

2.1 Golf Equipment Design

A typical golf course is comprised of 18 holes. Each hole includes a putting green, which has the shortest grass on a golf course and is where the hole/pin is located. Each hole also has a teeing area where a player will make their first stroke. The distance from the tee

to green will vary from hole to hole. Along this path is a shorter cut of grass, usually cut about half an inch tall, referred to as the fairway. This path also consists of hazards for the player to negotiate. This can include water, sand traps (bunkers), trees, and longer cuts of grass. Hence, it is preferred for a player to make subsequent shots from the fairway. There is no standardized course design; this makes every golf course unique. In 1938 the USGA and R&A, golf's two governing bodies, introduced a rule limiting players to 14 clubs. Therefore, to shoot the lowest score possible, club selection is important.

Most golfers use a unique club called a driver for their first shot. This club is designed for the player to hit the ball the farthest distance possible. This club features the largest clubhead and longest shaft in a set of clubs. Since this club is primarily used in the teeing area, the ball is elevated above the ground using a tee. Once the golfer is on or near the green, a club called a putter is used. A putter is designed to make short and slow swings to precisely roll the ball on the green. This club has the shortest shaft length and is usually the heaviest in a set of clubs. The vast majority of golfers include a driver and putter in their set of up to 14 clubs. The choice of the remaining 12 clubs varies from one golfer to another.

The main attributes of the club that affect how far a golfer can hit it are loft and shaft length. Loft is the angle between the clubface and the vertical plane. Static loft is measured with the club in an upright orientation. Dynamic loft is measured at the moment of impact. A typical driver has between 9-10 degrees of static loft. The shaft length for most drivers is close to the permitted 46 inch (1.16 m) maximum [10]. A set of clubs will usually have a number printed on each club. Generally, the lower numbered clubs have lower lofts and are designed to hit the ball a further distance. Thus, the number one is used for the driver. Higher numbered clubs are typically referred to as woods and irons. These clubs have increasing lofts and decreasing shaft length to reduce how far the ball will travel. To shoot the lowest possible score across 18 holes, selecting a set of clubs is important.

2.2 Golf Ball Impact Models

The collision between a golf club and ball occurs in under 0.5 ms and can accelerate the ball to speeds upwards of 80 m/s [7]. The contact forces between the ball and clubhead can exceed 10 kN. Impact models have led to advances in club design, resulting in players

being able to hit the ball farther and straighter. This section examines the major advances in golf impact modeling.

There are two approaches to modeling the impact behavior. The simplest method is to propel a golf ball into a rigid plate or fixed clubhead. These models are referred to as oblique impact models. Several researchers have developed models to predict the final velocities or contact forces. These experiments are highly repeatable and useful to evaluate equipment performance. The other approach is to simulate a clubhead striking a golf ball. Several researchers have conducted experiments using swing robots and human participants. The purpose of these models is to predict the launch conditions of the ball given the clubhead kinematics at the moment of impact. In this thesis, these models are referred to as clubhead impact models. These models can be combined with an aerodynamic model to simulate ball flight. This type of impact model is the aim of this research.

One of the longest held assumptions in this area of research is the free-body assumption, the idea that the clubhead behaves as a free body during impact. Cochran and Stobbs were the first to publish this in 1968 [11]. To demonstrate this principle, they constructed a 2 wood with a hinge connecting the shaft and the hosel. This hinge was designed to give away at impact. This hinged club resulted in a 2.3% decrease in distance compared to a standard club. Cochran and Stobbs suggested this discrepancy is due to the additional weight of the club. This experiment suggests the majority of energy transferred to the ball is from the inertia of the clubhead. This has given way to the free body assumption, which is utilized by many of the impact models discussed in this chapter.

2.2.1 Discrete Impact Models

Discrete impact models do not have a time domain. These models use the initial conditions of the system to predict the velocities after impact. Discrete models cannot be used to predict the intermediate states during the collision, nor the time varying contact forces. These models typically use the impulse-momentum (IM) principle and are often referred to as IM impact models. Impulse ($\vec{p}$) is a vector quantity and is defined as the time integral of a force applied to an object. The object's change in momentum (the product of mass and velocity) is equal to the applied impulse. This relationship can be derived by integrating Newton's second law with respect to time as shown in equations 2.1 and 2.2. By Newton's third law, when an impulse is applied to a body, an equal and opposite impulse

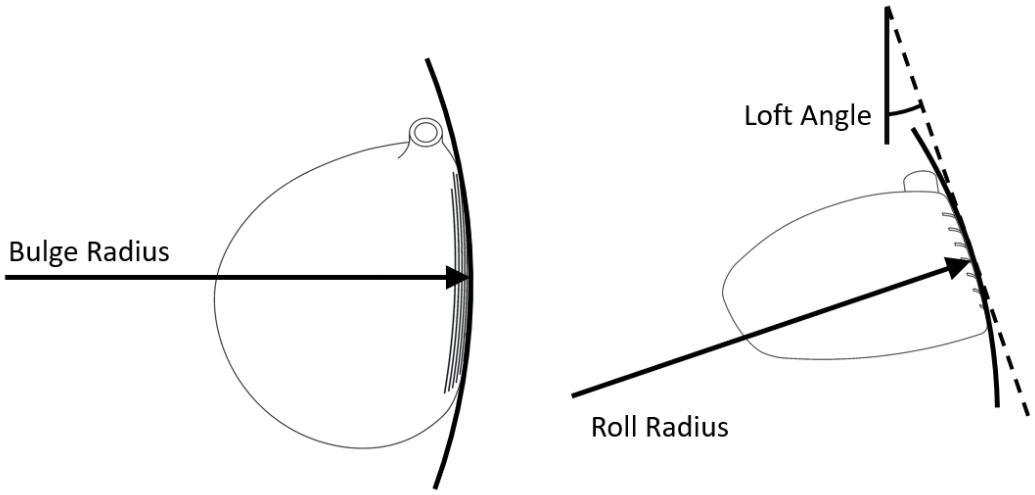

Figure 2.1: Diagram showing the loft, bulge radius, and roll radius of a driver clubhead.

is experienced. These relations are used to develop a system of equations for IM-based models.

$$\int \vec{F}\, dt \;=\; \int m\, d\vec{v} \tag{2.1}$$

$$\vec{p} \;=\; m\,(\vec{v}_{final} - \vec{v}_{initial}) \tag{2.2}$$

Fundamentally, all IM-based clubhead impact models treat the clubhead and ball as two free bodies. Since IM models ignore the duration of the impact, some assumptions are introduced. First, it is necessary to assume the collision occurs instantly. This implies that the positions of the clubhead and ball do not change during the impact. Subsequently, the change in velocity of both the clubhead and ball occurs instantaneously. Additionally, this implies both bodies are rigid, with negligible deformations. Finally, this leads to the assumption there is a single point of contact between the clubhead and ball. This point is where the impulse is applied. The impact duration of a typical drive is between 0.4-0.5 ms [12]. While these assumptions seem reasonable for a golf impact model, a high-speed camera will reveal just how compliant these objects can be. During the collision, a golf ball can compress to three quarters its original diameter [13]. The contact patch between the ball and club can be over 2 cm in diameter. Despite these observations, several researchers have shown IM models are reliable to predict golf shots [14, 15].

The first three-dimensional IM-based clubhead impact model was proposed by Winfield and Tan in 1994 [16]. This model was developed to predict the launch conditions and ball flight for a drive. Winfield and Tan used an ellipsoid to model the curved surface of a driver. This curvature is referred to as the bulge and roll radii. Bulge is the curvature about the vertical axis and roll radius is about the horizontal axis. Figure 2.1 illustrates the bulge radius, roll radius, and loft of a driver. An ellipsoid allows for these radii to be controlled individually. The impulse-momentum principles are applied to produce a set of linear equations. Each body has three transnational and three rotational degrees of freedom. As the collision is inelastic, conservation of energy cannot be applied. Winfield and Tan used a coefficient of restitution (COR) to account for the energy loss [16]. COR is frequently used to describe the efficiency of impacts. COR is defined as the ratio of relative velocity after and before the collision as shown in equation 2.3.

$$e\ (COR)\ =\ \frac{|Relative\ velocity\ after|}{|Relative\ velocity\ before|} \tag{2.3}$$

Using COR is also convenient as the rules of golf have imposed an upper limit of 0.83 to reign in distance. Lastly, Winfield and Tan proposed a pure rolling condition to generate two more equations. This is achieved by equating the tangential velocities at the point of contact. This yields a system of 15 linear equations to predict the launch conditions of the ball. The authors then used a golf ball aerodynamic model to predict ball flight and carry distance. To validate the model, Winfield and Tan used a swing robot to strike the middle of the clubface and compared the carry distance. This does not directly compare the predicted velocity or spin rate of the ball. While the model is 3D, predicting only centered strikes produces straight, 2D ball trajectories. The authors used this model to study the effect of driver loft on carry distance. In a later paper in 1996, Winfield and Tan used this model to predict off-centre hits [17]. The authors used this to optimize the curvature of the clubface to reduce the dispersion of mis-hits.

In 2001, Penner developed a 2D driver IM model using a similar approach to Winfield and Tan. The key differences are that Penner modeled a flat clubface and proposed the COR was a function of impact speed and loft [18]. Penner also proposed a ground model to predict the rollout of a drive. This model was used to optimize driver loft for various swing speeds. In a related paper, Penner updated this model to be three dimensional [15]. The driver clubface was represented using a cylinder, which gives a constant bulge radius and zero roll. For off-centre strikes, this produces sidespin, giving the ball a curved trajectory.

This model was used to determine the optimum bulge radius of a driver.

Many researchers have studied 2D oblique impacts and questioned the pure rolling assumption used by IM models. Chou *et al* conducted impact experiments with different surface treatments [19]. The authors found that for a typical driver loft, the surface finish does not significantly affect the spin rate. This supports the pure rolling assumption. Cross proposed a non-dimensional quantity referred to as the horizontal coefficient of restitution (e_t) [20]. The previous COR definition uses the normal velocity comments before and after the collision. The horizontal COR proposed by Cross uses the relative velocity at the point of contact in the tangential direction. For a 2D collision between a ball and rigid plate, the horizontal coefficient of restitution is defined by equation 2.4.

$$e_t = \frac{(v_t - \omega r_{ball})_{After}}{(v_t - \omega r_{ball})_{Before}} \tag{2.4}$$

In equation 2.4, v_t is the tangential velocity of the ball, ω is the angular velocity, and r_{ball} is the radius of the ball. If the numerator of equation 2.4 is zero, then the relative velocity between the ball and impact surface is zero. As a result, the horizontal COR is zero and the ball is in a state of pure rolling after impact. Cross performed several experiments with different types of sports balls and found that the horizontal COR can be either positive or negative. For collisions at a shallow angle of incidence or against a low friction surface, $e_t < 0$. This means the final angular velocity is less than assuming a pure rolling condition. Cross and other researchers refer to this behavior as slip. Additionally, there are certain conditions where $e_t > 0$. This means the ball spin is greater than assuming a pure rolling condition. Cross performed experiments using golf balls and found that premium golf balls can have a horizontal coefficient of restitution between 0.2-0.3 for 50° incidence angles. The authors refer to this behavior as the ball "gripping" the clubface. In subsequent papers, Cross and Dewhurst developed 2D golf impact models using this concept [21]. However, as the impact moves closer to perpendicular, e_t becomes closer to zero. Hence, for modeling the driver, the pure rolling assumption is widely accepted.

In 2015, Dewhurst observed that IM models under-predicted ball speed for strikes near the heel of the clubface [22]. The heel of the clubface is the side connected to the shaft of the club. The authors proposed adding 25% of the shaft's mass to the clubhead for heel strikes. This suggests a limitation of the free-body assumption and the effect of ignoring the shaft. In 2020, Danaei *et al* proposed an adjusted IM driver model to address these shortcomings [23]. This model is derived similarly to Winfield and Tan's model. Danaei *et*

al used toroidal geometry to model the clubface rather than an ellipsoid. The key difference to this model is the adjustments for certain model parameters. First, a small amount of mass is added to the clubhead to compensate for the free-body assumption. This will increase the model's predicted ball speed. The authors determined it was only necessary to add a few grams, significantly less than Dewhurst's suggestion. Second, to account for the deformations during impact, the ball center of gravity is moved. This creates a longer moment arm that reduces ball spin. These two adjustments were determined using an optimization process. The goal was to minimize the error between experimental measurements and the model's predicted launch conditions. While these adjustments are small, they have a significant effect on mean ball speed and spin error.

Several researchers have also developed IM-based models for putters. Lindsay *et al* developed a 2D putter model (vertical plane) to analyze launch angle and spin rates [24]. This was combined with a putting surface model to predict the path of the ball. Lindsay used this model to optimize putter loft and clubhead mass properties. Lambeth *et al* developed a 2D putter model (horizontal plane) to analyze off-centre hits [25]. This model demonstrated good agreement with experimental results supporting the free-body and pure rolling assumptions. The authors determined that moving a putter's CG forward reduces the offline distance for mis-hits.

2.2.2 Continuous Normal Force Models

Continuous impact models explicitly model the time-varying contact forces during the collision. Positions and velocities are determined by solving the differential equations of motion. Therefore, many assumptions used by discrete models are no longer needed. However, several continuous models still use the free-body assumption to model the clubhead. To study impact dynamics, it is a common practice to separate the contact forces into normal and tangential components. This section focuses on normal force models.

Many researchers have used Hertzian contact theory to model elastic collisions. Hertz developed an analytical solution for the stress distribution of an elastic sphere during contact. This theory suggests the normal force is proportional to the penetration depth raised to the $\frac{3}{2}$ power. To model inelastic collisions, Hunt and Crossley added a damping term that is proportional to the normal approach velocity [26]. This captures the loss of energy, providing the ability to model inelastic collisions. The Hunt-Crossley model for

normal force F_N, is shown in equation 2.5.

$$F_N = kx^{\frac{3}{2}} + d\dot{x}\,|x|^{\frac{3}{2}} \tag{2.5}$$

In equation 2.5, k is a stiffness parameter calculated using the material's Young's modulus and Poisson's ratio, and the sphere radius. d is a hysteretic damping parameter used to account for the energy lost during inelastic deformation. x is the penetration depth of the sphere and $\dot{x}$ is the normal approach velocity. $\dot{x}$ is positive during the compression phase and negative during the rebound phase of impact.

A similar approach to modeling this behavior is to use a system of non-linear springs and dampers. In 1994, Lieberman and Johnson proposed a five-parameter spring and damper model to predict normal impacts between a golf ball and rigid surface [27]. The parameters were identified using an optimization process to match the experimental normal force histories. In 2002, Cochran proposed a simpler two-parameter model with a spring and damper in parallel [28]. Equation 2.6 is the optimized normal force function proposed by Cochran.

$$F_N = kx\,|x|^{\frac{1}{2}} + d\dot{x}\,|x|^{\frac{1}{2}} \tag{2.6}$$

Cochran determined the exponents in equation 2.6 using experimental normal force measurements. The first term is the same as equation 2.5. The second term, which produces the damping force, is raised to the power of $\frac{1}{2}$ while in equation 2.5 it is raised to $\frac{3}{2}$ power. Cochran stated that this model is not accurate at slow impact speeds. Instead, the model is tuned for 40-55$\frac{m}{s}$ impact speeds, which is representative of a driver impact. Both models proposed by Cochran and Lieberman predicted that the COR decreases with increased ball speed. This aligns well with experimental studies and is one of the advantages of continuous models.

In 2007, Gonthier *et al* proposed a volumetric contact model designed to be computationally efficent for dynamic simulations [29]. The authors proposed a normal force that is proportional to the volume of intersection between the two bodies. This normal force is applied to the centroid of the contact area. This model is derived by considering the contact area as a bed of continuous springs. In 2018, McNally *et al* used this contact model with a Hunt-Crossly damping term to predict driver impacts [30]. Equation 2.7 is the volumetric normal force model.

$$F_N = kV\,(1 + d\dot{x}) \tag{2.7}$$

In Equation 2.7, k and d are stiffness and damping parameters. V is the volume of intersection. McNally *et al* calculated the volume of intersection using two spheres to represent the golf ball and clubface curvature. As the ball and clubhead are brought closer together, this volume of intersection increases exponentially. Similarly, Hertz' and Cochran's models state the normal force is proportional to $x^{\frac{3}{2}}$. Therefore, all three normal force models disused in this section follow a similar behavior.

2.2.3 Continuous Tangential Force Models

Coulomb friction is perhaps the simplest model for the tangential force between two surfaces in contact. This theory states the maximum tangential force is proportional to the normal force and applied in the direction opposite to relative motion. Several researchers have measured the friction coefficient for various golf balls and surfaces [31, 32]. The reported values in literature for the coefficient of friction range from 0.3-0.5 [31, 32]. Coulomb friction has been used in several Finite Element (FE) simulations of golf ball impacts. Chou *et al* developed a 2D FE model to study oblique impacts [19]. The authors compared the model to experimental results with good agreement. Tavares *et al* developed a 3D FE impact model with a multi-layer ball [33]. The authors demonstrated how ball construction influences the rebound angle and spin rate. Tanaka *et al* performed oblique impact experiments measuring ball velocity, contact forces, and ball compression [34]. This data was used to develop a FE ball model using a three-element linear solid model. The model was constructed with three layers to investigate the influence of the material's properties. The authors highlighted the importance of the hyperplastic and viscoelastic properties on the accuracy of the model. They also suggested experiments to identify these parameters. Several other FE models have been constructed using the standard linear model.

Several researchers have studied the tangential behavior during oblique impacts. In 2002, Cross performed several impact experiments with various sports balls against a rigid plate to measure the contact forces [20]. Cross found that for shallow angles of incidence, the ball slides through impact. The tangential force for this scenario is accurately predicted using Coulomb friction. Cross found that at higher impact angles, elastic balls do not transition to pure rolling during the collision. The measured tangential forces exhibited a periodic behavior. Golf balls typically demonstrated one force reversal cycle during impact, while tennis and basketballs could have several cycles. Cross concluded this periodic

behavior is caused by the ball vibrating in the tangential direction. This tangential force phenomenon is supported by some FE models as well [19].

There are a few impact models that predict this periodic tangential force behavior that are not FE models. In 1976, Maw *et al* proposed an analytical model (referred to as Maw) for the oblique impact of an elastic sphere [35]. They modelled the contact area as a series of concentric rings using Hertzian contact theory to predict normal stresses and displacements. While in contact, these rings can either be sticking to the surface or sliding, which the authors describe as grip-slip behaviour. When a ring grips the surface, the surface of the ball is displaced storing elastic energy. This storing and release of energy causes the vibrations observed in the tangential force histories. Cross compared the experimental force histories with the Maw model and found good agreement [20]. In 2010, Stronge *et al* proposed a similar impact model to capture this periodic tangential force behavior [36]. This model is more general as it designed for any geometry. The authors model the bodies as inelastic with a discrete element model at the point of contact. This model predicts similar force histories compared to the Maw model.

Other studies have been conducted to validate the Maw model specifically for predicting golf impacts. The sports governing bodies (USGA and R&A) were interested in understanding the factors that affect the spin rate of a golf shot [37]. They considered a variety of club surface treatments, groove geometries, and ball types. As the sports governing body, they were concerned that new designs are producing higher spin rates and making the game easier. They conducted several impact experiments shooting golf balls against rigid plates and measuring the contact forces. The authors found the Maw model demonstrated strong agreement with the experimental results. The drawback of the Maw model is that it only predicts perfectly elastic collisions. In 2020, Henrikson *et al* performed similar impact experiments [32]. The authors found that reducing the initial velocity inputted into the Maw model produced better predictions for the outbound velocity. This is to compensate for the Maw model being perfectly elastic.

To capture the tangential force reversal, McNally *et al* proposed a two-layer ball model [30]. This model consists of an inner core connected to an outer layer by a 3D rotary-spring damper. During the impact, the outer layer sticks to the contact surface. Then the inner layer rotates, storing energy in the spring. Tuning the spring stiffness will adjust the natural frequency and affect the degree of tangential force reversal. For predicting the contact forces applied to the outer layer, McNally *et al* used a continuous velocity-based

friction model proposed by Brown and McPhee [38]. The original friction model proposed by Brown and McPhee had terms for viscous friction and the stiction effect. For simplicity, McNally *et al* only used the first term of Brown and McPhee's model giving equation 2.8.

$$F_f = F_n \mu \tanh\left(\frac{4\ v_t}{v_{tr}}\right) \tag{2.8}$$

In equation 2.8, v_t is the relative velocity, F_n is the normal force, μ is the coefficient of dynamic friction, and v_{tr} is a parameter refereed to as the transition velocity. When v_t is greater than v_{tr} or exactly zero, this model is the same as Coulomb friction. However, using Coulomb friction in dynamic simulations can cause rapid oscillations at the contact point when the relative velocity is close to zero. This velocity based model is more suitable for dynamic simulations since the friction force gradually decreases when the relative velocity gets close to zero. This two-layer ball model is designed to capture the behavior observed in the Maw model and FE models, while being computationally less expensive.

Arakawa *et al* performed several oblique impact experiments with golf balls [13]. Using a high-speed camera, the contact area and spin rate was measured at several instants. Arakawa *et al* found Hertz contact theory adequately predicted the normal force. Arakawa *et al* proposed that the friction force is proportional to the normal force and time derivative of the contact area. This is expressed in equation 2.9.

$$F_f = \mu F_N + \mu\eta \frac{dA}{dt} \tag{2.9}$$

In equation 2.9, μ and η are contact parameters, however μ is not a friction coefficient. While it may seem unintuitive for the friction force to be dependent on the time derivative of the contact area, A, this does align with experimental observation. For golf impacts, the friction reversal typically occurs in the rebound phase. In this phase, $\frac{dA}{dt}$ is negative, which produces the friction reversal. However, this model is not a predictive impact model. The authors used experimental measurements of the contact area to solve this expression. Therefore, impacts with different initial conditions cannot be predicted.

2.2.4 Continuous Clubhead Impact Models

This section discusses continuous impact models that predict the initial launch conditions of the ball given the kinematics of the clubhead. Additionally, all the models discussed

in this section are 3D. Therefore, these models can be used to predict off-centre hits and estimate sidespin. These models can provide insights into the design and tuning of golf equipment.

In 2000, Iwatsubo *et al* developed a FE driver impact model [33]. The authors determined a high vertical moment of inertia (MOI) and shallow center of gravity (CG) depth reduced the offline distance for off-centre hits. In 2017, Wu *et al* developed an FE model to optimize a driver's clubface geometry [39]. It is known that a thin clubface will result in higher ball speeds. Equipment manufacturers refer to this as the trampoline effect. However, equipment design is limited by the USGA imposing a maximum COR of 0.83. Wu *et al* demonstrated that a variable thickness face can produce higher ball speeds across the clubface [39].

One of the longest held assumptions in this field of research is the free-body assumption. Tanaka *et al* were the first to develop a driver impact model with a flexible shaft [40]. The authors used a FE model for the ball, clubhead, and shaft. They determined including the shaft can reduce the predicted offline distance for off-centre hits. Cross and Dewhurst made a similar observation with IM-based models [21]. However, the shaft model proposed by Tanaka *et al* is not representative during a swing. The authors model the shaft as being fixed at the grip end and shooting a ball at the clubface. More recently, McNally *et al* developed a driver impact model with a flexible shaft using an analytical beam model [41]. Therefore, this model is considerably less computationally expensive compared to an FE model. The authors initialized the clubhead and shaft kinematics using data from elite golfers. This gives the shaft the correct angle and deflection at impact. The authors found including the shaft maintained higher clubhead speed through impact. In conclusion, these models suggest some limitations of the free-body assumption proposed by Cochran and Stobbs.

Using FE models to design golf equipment is a powerful tool; however, these simulations are tedious to run. There are some aspects of club design that require FE models. For example, designing a variable thickness clubface can only be achieved with a FE model. However, determining the optimal CG position or optimal loft angle can be done using analytical models or discrete IM-based models. Therefore, selecting a class of model depends on the analysis objectives.

2.3 Golf Turf and Soil

While a golf course may appear to be a large area of grass mowed at a few different heights, the design and construction is much more complex. The USGA spends millions of dollars researching every aspect of a golf course. From this research, guidelines are published for the construction and maintenance of golf courses. The main focus is to improve playing conditions while reducing operating cost. The fairway and rough is referred to as the general area. This covers the majority of a course and is where a player will make most of their strokes. To model the behaviour of shots from this area, it is important to have an understanding of their construction.

The USGA recommends a turf grass height between 0.38"- 0.5" for fairways [42]. The species of grass varies from region to region. In North America the most common types are bent, Bermuda, fescue, and ryegrass [43]. To reduce operating cost, many golf courses use pesticides and growth regulators. The USGA demonstrated that this results in thinner grass, which reduces mowing frequency and grass clippings from mowing [42]. The conditions of the rough are more varied. The grass turf height is typically 2.5 inches; however, it can be over 4 inches to make a course more difficult [44]. It is common practice to over-seed the rough area to make it fuller and lusher [44]. This makes shots from this area harder to hit accurately.

In 2015, Green published a study that evaluated the benefits of rolling and topdressing golf course fairways [45]. Top dressing is a process where a thin layer of sand is spread across the turf. The author found that rolling and top dressing fairways decreased the need for fungicide (a pesticide for fungus) [45]. Additionally, this improved playing conditions by increasing the shear resistance of the soil. This results in the ground being firmer, causing the ball to bounce higher and roll farther. Also, these treatments are beneficial for high traffic areas as less damage is done by golf carts and equipment traversing. Based on these findings, the USGA endorses topdressing up to 0.5" per year for fairways [46]. Soil particle analysis shows the top layer of turf can contain as much as 50% sand [45].

2.3.1 Golf Ball and Turf Models

Several researchers have studied the collision between a golf ball the turf. Typically, the goal is to determine the final resting position of the ball, as this is where a player will make

their next stroke. The models discussed here are for the behavior of fairways and greens.

In 1994, Haake proposed several analytical contact models for the impact between a golf ball and putting green [47]. Haake performed normal impact experiments by firing golf balls onto putting greens and measuring the velocity after impact. Haake initially modeled the normal force using a Kelvin-Voigt model. The author found that the Kelvin-Voigt model predicted forces that were too large at the beginning of the impact. Haake proposed a modified model where the normal force was proportional to the area of contact between the ball and green. This modified normal force model caused the ball to penetrate further into the green's surface, which aligned better with experimental observations. Haake used this normal force model to develop an oblique impact model. This model used Coulomb friction to model the tangential forces. Haake used this model to run several predictive simulations to study the effects of green conditions and ball velocity.

In 2002, Penner proposed a 2D oblique impact using the principles of impulse and momentum [48]. Similar to the clubhead impact models, Penner used a COR to capture the loss in energy. Here the effect of the COR decreasing with impact speed can not be ignored. While Penner noted that the turf used to collect data was relatively soft, the measured COR ranged from 0.12-0.5. This model is very versatile as it was used to predict the rollout from drives down to wedge shots landing on a green and spinning backwards. Overall, this model agrees well with experimental observations. Penner determined that descent angle is the most important landing condition related to the rollout of the ball. In 2021, the USGA was interested in predicting the rollout of a drive and the factors that influence this behavior [49]. The authors proposed a simple linear relation in which rollout is a function of descent angle. This model has good agreement among top players.

2.3.2 Terrain Mechanics and Measurement of Soil Properties

Soil mechanics is a field of science and engineering that studies the mechanical behavior of soils. There are many similarities to solid mechanics. The main difference is that soils are a heterogeneous mixture of materials consisting of different particle sizes and shapes. The field of terramechanics (terrain mechanics) applies soil mechanics to predict the performance of off-road machinery. For decades, researchers have developed models of vehicles traversing terrain and earth moving equipment. This section reviews some of the methods and soil models used in this field.

As in solid mechanics, normal stress and shear stress are also used to describe the loading conditions of soils. In the 1950s, Bekker pioneered a device called a bevameter to measure terrain properties [50]. This device performs a pressure-sinkage test measures the response to normal stress. A separate shear test is performed to measure the shear-displacement relationship. This consists of a disc that is pressed into the ground and rotated. Shear stress is measured by the torque and angle of the disc. Many other researchers have developed mobile bevameters to measure terrain properties in the field. While other test methods have been used to measure soil properties, the adoption of Bekker's method is beneficial. There are several published Bekker parameters for different regions, climates, and soil types.

The first empirical model of the pressure-sinkage behavior was published by Bernstein in 1913 [51]. Bernstein proposed an exponential relationship for normal pressure, P, shown in equation 2.10. In equation 2.10, z is the penetration depth (sinkage), k is the sinkage modulus, and n is the sinkage exponent.

$$P = k\ z^n \tag{2.10}$$

Several other models have been proposed that follow a similar exponential form. Bekker proposed equation 2.11 for the pressure-sinkage behavior of soils. In equation 2.11, the terms inside parentheses are constants, k_C and k_ϕ are soil parameters, and b is the smaller dimension of the contact area.

$$p = \left(\frac{k_C}{b} + k_\phi\right) z^n \tag{2.11}$$

Becker demonstrated that this relationship independent of the size or shape of the testing implement. The only limitation is the object's aspect ratio can not be greater than 5 (length divided by width). There are several published parameters for this model measured using bevameters. Table 2.1 shows soil parameters from a variety of regions across North America [50]. This shows that soil parameters vary dramatically based on the composition, location, and compaction.

The other important mechanical property needed to model terrain behavior is the shear resistance. In soil mechanics, the Mohr-Coulomb failure criterion is commonly used to model the maximum shear strength of soils [50]. Equation 2.12, τ_{max} is the shear stress that will cause the soil to fail, c is a soil parameter for the cohesion of the soil, σ is the

Table 2.1: Typical terrain properties found in North America [50]

Terrain Type	n	$k_c \left(\frac{kN}{m^{n+1}}\right)$	$k_\theta \left(\frac{kN}{m^{n+2}}\right)$
North Gower loam	0.73	41.6	2471
Rubicon sandy loam	0.66	10.5	880
Greenville loam	1.01	66	4486
Upland sandy loam	0.85	26.8	1522
LETE sand	0.61	1.16	475
Loam - medium compaction	1.03	16.5	6880
Loam -firm compaction	1.20	29.8	13900

normal pressure acting on the surface, and Φ is a soil parameter referred to as the angle of internal shearing resistance.

$$\tau_{max} = c + \ \sigma \tan \Phi \tag{2.12}$$

Similar to solid mechanics, under small strains, soils experience elastic deformation. In this region, the shear resistance is less than equation 2.12. However, it is common to model soil as a perfectly plastic medium [50]. Therefore, any motion is resisted by the maximum shear stress of the soil. This assumption also ignores the elastic recovery behavior as well. In terramechanics, this assumption is reasonable as the strains due to earth moving equipment are very large.

These mechanical properties are used to develop several different models to predict vehicle performance. The simplest methods are empirical models. The US Army Corps of Engineers developed empirical models for wheeled and tracked vehicles [52]. Empirical models can not estimate stresses or sinkage. These models are intended to be a quick reference on a go or no-go basis. Parametric models have also been developed to predict the performance of wheeled and tracked vehicles [50, 53]. These models can predict the forces acting on the wheel and the torque required.

In the 1990s, the increase in computing power allowed for FE models to be used for vehicle performance. To capture the non-homogenous characteristics of soil, these models give different mechanical properties to different elements [50]. Early models used non-linear elements. Over the years, a number of different constitutive elements have been developed.

However, this does not entirely escape the fact that FE models are inherently designed for materials that can be treated as a continuum. As a result, FE terrain models do not predict large displacements, referred to as soil flow.

More recently, discrete element (DE) models of terrain have been developed to address the limitations of FE models [50]. DE models represent terrain as a group of individual elements. These elements have different material properties, shapes, and sizes to reflect the non-homogenous characteristics of terrain. However, with a DE model, these elements are free to move. Displacements occur from contact forces due to the vehicle or neighbouring elements. The forces between discrete elements are typically modeled using non-linear springs and dampers based on Hertzian contact theory. This process is very computationally demanding.

2.4 Opportunities for Improvement

There are many opportunities to improve the models discussed in this chapter. First, the opportunities pertaining to modeling golf impacts are discussed. From section 2.2, there are some gaps in the published research. These are some of the potential areas of new research:

- Develop and validate a parameterized iron impact model using the impulse-momentum principle. Several driver IM models have been published, experimentally validated, and used to optimize driver designs. However, irons are constructed differently compared to a driver. These clubs have a higher loft angle, lower moment of inertia, and a center of mass closer to the clubface. It would be beneficial if IM models can be applied to design and optimize clubs besides a driver.

- There are several published contact models to predict collisions between a ball and rigid plate. These experiments are valuable as they can provide insight into the contact forces, which is useful to validate contact models. It would be valuable if these models can be applied to predict a collision between a moving clubhead and a golf ball.

- Several impact models assume a pure rolling condition between the ball and clubface. On the other hand, many experimental studies have shown that this is not always

the case. This will affect the predicted launch angle and spin of the ball. Therefore, opportunities exist to develop impact models that do not strictly enforce a pure rolling condition.

- Currently, most impact models assume the ball is hit off a tee. However, this is only allowed for the first shot on a given hole. It would be valuable to model clubs being hit off the ground. When hitting off the ground, elite golfers will generally hit the ball first. However, it is common for amateur golfers to hit the ground before the ball. Therefore, the ground reaction force between the clubhead and ground could affect the trajectory of the ball. Including ground reaction forces would allow this type of mishit to be modeled.

Chapter 3

Golf Club and Ball Impact Modeling

One of the main goals of this work was to evaluate different contact models to predict the initial launch conditions for a golf shot. The models proposed in this section are evaluated using experimental data for driver and 7-iron shots. To compare these models, the accuracy of the predicted launch conditions and computational efficiency will be considered. These criteria were chosen because these models are intended to be used for club design and optimization. Hence, the model needs to be fast as it may need to simulate thousands of impacts.

3.1 Impulse-Momentum Models

This section explains the general methodology behind a golf impulse-momentum (IM) model. The following subsections discuss the different IM models used for this comparison. IM models predict the launch conditions of a golf shot by applying the principles of linear and angular impulse-momentum. The typical approach is to model the clubhead and ball as two free bodies as discussed in Chapter 2. The clubhead is prescribed an initial velocity and the goal is to predict the final velocity of the ball. Due to the construction of IM models, several assumptions are imposed. First, IM models are discrete with respect to time, which implies that the collision is instantaneous. This leads to the assumption that neither body translates nor rotates during impact. Therefore, the contact between the clubhead and ball occurs at a single point. Furthermore, this implies that the change in velocity for both

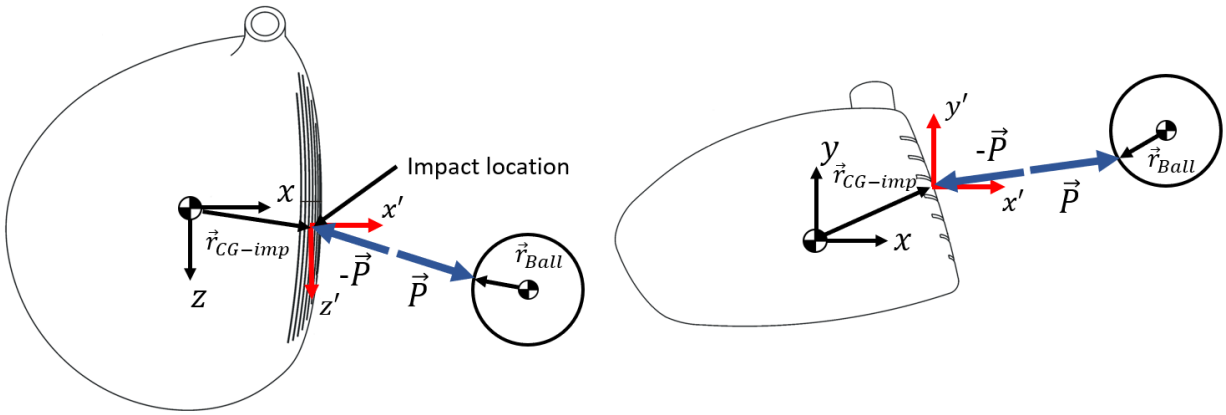

Figure 3.1: Free body diagram of the clubhead and ball.

the clubhead and ball occurs instantly. Finally, to model inelastic collisions, a coefficient of restitution (COR) is imposed along the axis normal to the clubface.

To construct the impact model, a system of equations is derived relating the velocities of each body before and after the collision. The ball and clubhead are modeled as free bodies as shown in figure 3.1. Each body has 3 translational and 3 rotational degrees of freedom. This gives 12 unknown velocity components after the collision. An impulse, $\vec{P}$, is applied to each body at the point of impact as shown in figure 3.1. Impulse is the integral of an external force with respect to time and is defined by equation 3.1. Therefore, this quantity is related to the change in a objects velocity. As per Newtons third law, a pair of impulses of equal magnitudes but opposite directions are applied to the ball and clubhead. Impulse is a vector quantity, bringing the total number of unknowns to 15. Velocities are measured at the centre of mass for each body. The reference frame $x'y'z'$ is moved to the point of contact and x' is along the normal clubface axis.

$$\vec{P} = \int \vec{F}\, dt \tag{3.1}$$

The following equations describe the change in linear and angular velocity for the clubhead. The clubhead properties are denoted by the subscript c. In equation 3.2, m_c is the clubhead mass and $\vec{v_c}$ is the clubhead velocity. In equation 3.3, I_b is the inertia tensor and ω_c is the angular velocity of the clubhead. As shown in figure 3.1, $\vec{r}_{CG_imp}$ is a vector from the clubheads center of gravity (CG) to the point of impact on the clubface.

$$m_c\vec{v}_{c_i} \; - \; \vec{P} \; = m_c\vec{v}_{c_f} \tag{3.2}$$

$$I_c\vec{\omega}_{c_i} \; - \; \vec{r}_{CG_imp} \times \; \vec{P} = \; I_c\vec{\omega}_{c_f} \tag{3.3}$$

Equations 3.2 and 3.3 are vector equations. This produces 6 scalar equations. Similarly, applying this process to the ball gives 6 additional equations. The ball properties are denoted by the subscript b. In equation 3.4, m_b is the mass and $\vec{v_b}$ is the velocity of the ball. In equation 3.5, I_b is the inertia tensor and ω_c is the angular velocity of the ball. Finally, $\vec{r}_{ball}$ is a vector from the ball CG to the point of impact.

$$m_b\vec{v}_{b_i} \; + \; \vec{P} \; = m_b\vec{v}_{b_f} \tag{3.4}$$

$$I_b\vec{\omega}_{b_i} \; + \; \vec{r}_{ball} \times \; \vec{P} = \; I_b\vec{\omega}_{b_f} \tag{3.5}$$

The right-hand side of equations 3.2-3.5 are the respective momenta just after the collision. Equations 3.4 and 3.5 can be simplified. The first term will be zero since the ball is initially at rest. To solve this system of equations, three more equations are needed. Since the collision is inelastic, energy is not conserved. The coefficient of restitution (COR) is a dimensionless quantity for the energy lost during a collision. This is applied along the x-axis of the local reference frame $x'y'z'$ (along the clubface normal).

$$e \; = \; \frac{-\left(\vec{v}_{imp,c_f} \; - \; \vec{v}_{imp,b_f}\right) \cdot \hat{\imath}'}{\left(\vec{v}_{imp,c_i} - \; \vec{v}_{imp,b_i}\right) \cdot \hat{\imath}'} \tag{3.6}$$

In equation 3.6, $\hat{\imath}'$ is the unit vector of the local impact reference frame. The subscript 'imp' denotes these velocities are at the point of contact instead of the object's CG. These velocities are calculated using equations 3.7 and 3.8, which are for rigid body motion.

$$\vec{v}_{imp,c} \; = \; \vec{v}_c \; + \vec{\omega}_c \times \vec{r}_{CG_imp} \tag{3.7}$$

$$\vec{v}_{imp,b} \; = \; \vec{v}_b \; + \vec{\omega}_b \times \vec{r}_{ball} \tag{3.8}$$

Lastly, equations 3.9 and 3.10 impose a pure rolling condition. This is applied by equating the ball and clubhead tangential velocity components after the collision.

$$\left(\vec{v}_{imp,c_f} - \vec{v}_{imp,b_f}\right) \cdot \widehat{j'} = 0 \tag{3.9}$$

$$\left(\vec{v}_{imp,c_f} - \vec{v}_{imp,b_f}\right) \cdot \widehat{k'} = 0 \tag{3.10}$$

This produces a set of 15 Scalar equations to solve for the final velocity componets of the ball and clubhead. Most IM-based models follow a similar derivation although there are some differences. Winfield and Tan developed an IM model that represents the clubhead using a 3D ellipsoid [16]. This is to capture the curvature of a driver's clubface referred to as bulge and roll. Penner proposed an IM-based driver model with flat clubface geometry [15]. Penner also proposed a linear relationship between COR and clubhead speed [15]. Danaei *et al* proposed an IM model that used a torus to represent the bulge and roll radii of a driver [23]. All the models considered in this chapter will assume a constant COR. The driver models will use a toroidal geometry, while the iron models will use planar geometry for the clubface.

3.1.1 Adjusted Impulse-Momentum Model for Drivers and Irons

This model proposed by Danaei *et al* makes two adjustments to physical model parameters to improve accuracy [23]. First, a small amount of mass is added to the clubhead mass. The Authors found this improved ball speed error without effecting spin. This additional mass is intended to compensate for neglecting the shaft. The second adjustment is a small translation to the ball's center of gravity (CG). The authors found moving the CG slightly downwards improved spin accuracy [23]. This adjustment is motivated from deformations of the ball during impact. The original paper outlines an optimization approach to identify these adjustments using experimental data. An objective function was created that reduced the mean square error for the linear and angular velocities of the ball [23].

To implement this model, all the equations presented in Section 3.1 still apply. The additional clubhead mass is added to the parameter m_c. The adjustment to ball CG is achieved by changing $\vec{r}_{ball}$ which is the vector from the ball's CG to the point of impact. This gives four variables to be optimized later. The optimization method and objective function used is outlined later in section 3.1.3.

3.1.2 Cross and Dewhurst Model Extend for Drivers and Irons

Cross and Dewhurst introduced a non-dimensional quantity referred to as the "tangential coefficient of restitution" [21]. This parameter allows for a certain amount of slip to occur at the point of contact. Therefore, it can be considered as a slip ratio. This replaces the pure rolling assumption used by the other IM based models. The original model is derived for 2D impacts. Here the model is extended to predict 3D impacts between two rigid bodies. Compared to the model outlined in section 3.1, equations 3.9 and 3.10 are modified to allow a prescribed amount slip between the clubhead and ball. This produces the following two equations to describe this behavior.

$$e_y = \frac{-\left(\vec{v}_{imp,c_f} - \vec{v}_{imp,b_f}\right) \cdot \hat{\jmath}'}{\left(\vec{v}_{imp,c_i} - \vec{v}_{imp,b_i}\right) \cdot \hat{\jmath}'} \tag{3.11}$$

$$e_z = \frac{-\left(\vec{v}_{imp,c_f} - \vec{v}_{imp,b_f}\right) \cdot \hat{k}'}{\left(\vec{v}_{imp,c_i} - \vec{v}_{imp,b_i}\right) \cdot \hat{k}'} \tag{3.12}$$

The numerator of equation 3.11 is the relative velocity between the ball and clubhead after impact, measured along the y' axis. Similarly, equation 3.12 is the relative velocity along the z' axis. Therefore, if these coefficients are set to zero, it is equivalent to a pure rolling condition. Likewise, if the slip ratio is greater than zero, the final ball spin is greater than assuming a pure rolling condition.

From 2D experiments, the authors report horizontal COR values ranging between -0.2 and 0.2 [21]. These values depend on the impact velocity, angle of incidence, coefficient of friction, and even the specific brand of golf ball used. For this 3D model, the slip ratio may be different in the horizontal and vertical directions. A golf club has a series of parallel grooves indented into the clubface. Therefore, the slip parameters e_y and e_z are left as variables to be optimized later.

3.1.3 Experimental Validation

Experimental data was collected by a golf equipment manufacturer. The data consists of 550 drives and 120 7-iron shots by elite level golfers. The golf shots were recorded with an 8 camera motion capture system (Nexus, Vicon, Oxford, UK). This system measured the

club kinematic data. The launch conditions of the ball were recorded using a commercial launch monitor (GC2, Foresight Sports, San Diego, CA, USA) . The clubhead velocity and position just before impact are used as the initial state for the models. This data was used to identify model parameters and evaluate the accuracy of these models. The physical properties of both clubheads and the golf ball are provided in table 3.1.

Table 3.1: Properties of the clubheads and ball.

Parameter	Driver	7-Iron	Description
m_c	204	264	Mass of the clubhead (g)
$\vec{r}_{CG-CF}$	$\begin{bmatrix}40.8 & 11.4 & 1\end{bmatrix}$	$\begin{bmatrix}3.61 & 4.85 & 1.12\end{bmatrix}$	Vector from CG to centre of the the clubface in xyz frame (mm)
I_{club}	$\begin{bmatrix}2843 & -733 & 530.2\\ -733 & 5679 & 0.5\\ 530.2 & 0.5 & 4085\end{bmatrix}$	$\begin{bmatrix}2752 & -51 & -53\\ -51 & 2889 & -429\\ -53 & -429 & 576.6\end{bmatrix}$	Clubhead inertia matrix about the xyz frame ($g \cdot cm^2$)
Loft	9.8	30.5	Loft angle (°)
Bulge	305	∞	Bulge radius (mm)
Roll	305	∞	Roll radius (mm)
m_{ball}	45.9	45.9	Mass of the ball (g)
r_{ball}	21.3	21.3	Radius of the ball (mm)
I_{ball}	$83.36I_{3\times3}$	$83.36I_{3\times3}$	Inertia matrix of the ball ($g \cdot cm^2$)

The impact models discussed in the previous sections have unique parameters that will affect the predicted launch conditions. An optimization approach is used to identify these parameters. Equation 3.13 is the cost function to be minimized.

$$C = \sum_{j=1}^{n}\left[\sum_{i=1}^{5}\frac{1}{n}\frac{|x_{Sim,i,j}-x_{Exp,i,j}|}{mean\left(x_{Exp,i,1}:x_{Exp,i,n}\right)}\right] \tag{3.13}$$

where $x_{i,j}$ is the launch conditions of the ball. $x_{Sim,i,j}$ are the simulated launch conditions of the ball and $x_{Exp,i,j}$ are the measured experimental values. j indicates the launch conditions for a particular shot of n total shots. The index i is for each launch condition

which has five possible values: ball speed, vertical launch angle, horizontal launch angle, backspin, and sidespin. The numerator of equation 3.13 is the absolute difference between the simulated launch condition and the experimental measurement. This is divided by the experimental mean to balance the weighting of each error term.

The optimization for parameter identification was completed in MATLAB (2021b). This presents several challenges due to the non-linearity of the problem. First the genetic algorithm was used to thoroughly search the solution space. This method repeatedly modifies a population of solutions. Random number generation is used to select the next generation. This method prevents the solution from settling at a local minimum. However, the method is also very inefficient. For this problem a population size of 200 was chosen. After 100 generations, the top five results from the current population are further optimized using MATLAB's fmincon function. This is a gradient based optimization method. Therefore, the results can be affected depending on the initial parameters. The best result from this process is used as the model parameters.

3.1.4 Results and Discussion

Table 3.2 summarizes the accuracy of the base impulse-momentum model outlined in Section 3.1. This model has no adjustments and assumes a pure rolling condition between the ball and club face. Table 3.2 lists the experimental mean absolute error for each launch condition. The accuracy of these models is evaluated by calculating the mean absolute error and standard deviation between the measured launch conditions. The percent error relative to the experimental mean is shown in parentheses in Table 3.2.

From table 3.2, the predicted ball speed is the most accurate launch condition for both models. The normalized mean absolute error is 1.18% for the driver model and 2.55% for the 7-iron model. Ball speed is arguably the most important launch condition when analyzing the performance of a club due to the industry's focus on distance. Launch angle and backspin have similar normalized errors of less than 10% for both clubs. The azimuth (horizontal launch angle) and sidespin normalized mean errors are much larger. However, the absolute errors are similar in magnitude compared to the vertical launch angle and backspin errors. The normalized errors for sidespin and azimuth appear larger mostly due to the experimental mean values being relatively small.

Table 3.3 summarizes the results for both clubs using the adjusted IM-based models

Table 3.2: Mean experimental value, mean absolute error, standard deviation and average CPU time per simulation for the standard IM models.

	Driver			7-Iron		
Ball	Exp.	MAE	STD	Exp.	MAE	STD
Speed (mph)	158.9	1.87 (1.18%)	1. 31(0.77%)	117.0	2.98 (2.55%)	2.62 (2.24%)
Launch (deg)	14.5	0.71 (4.90%)	0.47 (3.03%)	18.9	1.16 (6.17%)	0.93 (4.92%)
Azimuth (deg)	2.19	0.79 (35.6%)	0.47 (21.9%)	2.19	0.96 (43.7%)	0.55 (25.1%)
Backspin (rpm)	2980	224 (7.50%)	248 (8.66%)	6487	632 (9.70%)	425 (6.55%)
Sidespin (rpm)	490	158 (32.3%)	191 (35.3%)	681	493 (72.3%)	420 (61.7%)
Avg. CPU Time		0.552 ms			0.583 ms	

proposed by Danaei *et al* Table 3.3 also records the model parameters identified through the optimization process. This is the mass added to the clubhead and the change in ball CG.

Comparing tables 3.2 and 3.3 reveals ball speed error is reduced with these adjustments. This is mainly attributed to the additional clubhead mass. This increases ball speed for all shots. From the optimization process, 2.54 grams were added to the driver model and 10.1 grams were added to the 7-iron model. This additional mass can be attributed to the iron shaft being heavier, at 104 grams compared to 60 grams for the driver shaft. Furthermore, the iron shaft is stiffer and shorter compared to the driver shaft. As for the adjustment to the ball center of gravity, both models moved the CG down and towards the heel of the club. However, the iron model also moved the ball CG closer to the clubface. These adjustments reduced the vertical launch, horizontal launch, backspin, and sidespin errors for both models. In conclusion, these adjustments do have a meaningful impact on the accuracy of the model.

Table 3.4 summarizes the results for the driver and 7-iron models using Cross and Dewhurst's' IM-based model. Table 3.4 also shows the horizontal coefficients of restitution identified from the optimization process.

Comparing tables 3.2 and 3.4, the ball speed errors with the Cross and Dewhurst models are similar to the standard IM models. This is expected because the changes in equations 3.11 and 3.12 only affect the direction tangential to the clubface. The improvements of

Table 3.3: Mean absolute error, standard deviation and model parameters for the adjusted IM models.

	Driver		7-Iron	
Ball	MAE	STD	MAE	STD
Speed (mph)	1.51 (0.95%)	1.27 (0.81%)	2.31 (1.97%)	2.28 (1.95%)
Launch (deg)	0.68 (4.68%)	0.50 (3.45%)	1.12 (5.93%)	0.99 (5.24%)
Azimuth (deg)	0.78 (35.6%)	0.49 (22.4%)	0.86 (39.3%)	0.53 (24.2%)
Backspin (rpm)	213 (7.15%)	257 (8.62%)	568 (8.75%)	363 (5.53%)
Sidespin (rpm)	150 (30.6%)	188 (38.3%)	340 (49.8%)	243 (35.7%)
Δ Mass (g)	2.54		10.10	
Δ CG_{Ball} (mm)	(0, -0.482, -0.068)		(-0.395, -0.182, -0.071)	
Avg. CPU Time	0.561 ms		0.604 ms	

the Cross and Dewhurst model are observed in the launch direction and spin error. For the driver, the optimized horizontal coefficients of restitution are close to zero. Therefore, the system is close to a pure rolling condition and the launch conditions are similar to the standard IM model. For the 7-iron model, table 3.4 shows a 141 rpm improvement to mean absolute sidespin compared to the standard model. The optimized coefficients of restitution for the iron models are greater than zero. This means the final ball angular velocity is greater compared to a pure rolling condition.

While the relative errors for sidespin and azimuth are large, a considerable portion of this error can be attributed to the data collection method. The club kinematics were recorded at 720 Hz. The driver has an average clubhead speed of 50 m/s. As a result, the position of the clubhead changes about 7 cm per frame at the bottom of the downswing. Therefore, to estimate the conditions at the moment of impact requires extrapolating the data. Here the two points before impact were used with a linear extrapolation method. Consider that the clubface can rotate between 3-4°per frame. Therefore, it is reasonable that the predicted angle at impact can be off by a few tenths of a degree. By comparison, the mean horizontal launch angle error is 0.78°. Hence, extrapolation errors are a limiting factor to quantify the accuracy of these models.

In conclusion, the modifications proposed by Danaei *et al* and Cross and Dewhurst,

Table 3.4: Mean absolute error, standard deviation and model parameters for the Cross and Dewhurst IM models.

	Driver		7-Iron	
	MAE	STD	MAE	STD
Speed (mph)	1.85 (1.17%)	1.37 (0.86%)	2.86 (2.44%)	2.49 (2.13%)
Launch (deg)	0.68 (4.71%)	0.50 (3.45%)	1.06 (5.12%)	1.07 (5.66%)
Azimuth (deg)	0.81 (37.5%)	0.48 (21.9%)	0.94 (42.9)	0.58 (26.5%)
Backspin (rpm)	219 (7.50%)	257 (8.62%)	583 (8.99%)	373 (5.75%)
Sidespin (rpm)	149 (30.2%)	176 (35.7%)	352 (51.7%)	250 (36.7%)
(e_y, e_z)	(-0.0103, -0.0151)		(0.0183, 0.0423)	
Avg. CPU Time	0.563 ms		0.621 ms	

demonstrated meaningful improvements to the accuracy of the standard golf IM impact model. Both models demonstrated similar improvements to the predicted ball spin and launch direction. However, the adjusted IM model proposed by Danaei *et al* was able to reduce mean ball speed error by approximately 0.5 mph. This is due to the variable mass added to the clubhead. Therefore, the adjusted IM model is the best IM model for predicting driver and 7-iron shots.

3.2 Continuous Models

Continuous impact models have a time domain and predict the contact force histories of the collision. Consequently, the assumptions introduced for IM models are no longer imposed as the clubhead and ball follow Newton's laws of motion. In this section, three different contact models are developed to predict the contact forces during a golf shot. By applying the differential equations of motion, the linear and angular velocity of the golf ball is predicted. These contact models are used in a free-clubhead impact model for a driver and 7-iron. These models were developed in Maplesim, version 2022.1 (Maplesoft, Waterloo, Canada), which is a multi-body dynamic simulation software.

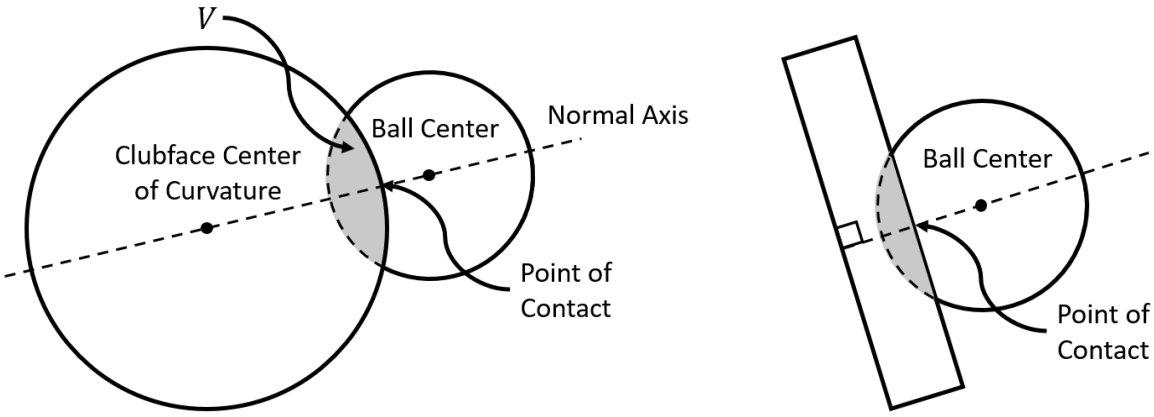

(a) Sphere-sphere volume of intersection. (b) Sphere-plane volume of intersection.

Figure 3.2: Volume of intersection for normal force model.

3.2.1 Two-Layer Ball with Volumetric Contact Model for Drivers and Irons

This model proposed by McNally *et al* [30], features a two-layer ball to capture the tangential force reversal observed in experimental studies and FE models. The inner core is connected to the outer cover with a rotary spring-damper. The thickness of the outer layer is left as a variable for the optimization process. Both the inner and outer components will have mass and inertia properties assuming a uniform density. Additionally, the spring stiffness and damper rate are left as variables to be optimized latter.

This model proposed by McNally *et al* is unmodified for driver impacts. However, for iron shots the normal force model is modified to reflect the difference in clubface geometry. The driver model calculates the volume of intersection (V) using two spheres to represent the curvature present on a driver's clubface. With the normal force direction intersection the center of these spheres. The volume of intersection and normal axis is illustrated in figure 3.2.

The iron model will calculate the volume of intersection using a sphere and plane to represent the flat clubface of an iron. The normal force axis is perpendicular to the plane and through the center of the ball. This model does not consider shots that hit on the edge of the clubface or on the hosel. Therefore, the experimental impact data used to

validate these models have these types of extreme mishit shots removed. As in the original model proposed by McNally *et al* [30], the normal force is calculated using the volumetric contact model proposed by Gonthier and McPhee [54]. To make the collision inelastic, a Hunt-Crossley damping term ($d\dot{x}$) is added as shown in equation 3.14.

$$F_N = kV + d\dot{x}kV \tag{3.14}$$

In equation 3.14, k is a stiffness parameter and d is the Hunt-Crossley Damping parameter. V is the volume of intersection and $\dot{x}$ is the normal approach velocity measured along the normal axis in figure 3.2. Equation 3.14 is used for both driver and iron models. Finally, the continuous velocity-based friction model, proposed by Brown and McPhee [38], is used for the tangential force. In the model proposed by McNally *et al* [30], only the dynamic friction component is used. This gives equation 3.15 for the tangential force.

$$F_f = F_n \mu \tanh\left(\frac{4\ v_t}{v_{tr}}\right) \tag{3.15}$$

In equation 3.15, v_t is the instantaneous relative velocity at the point of contact. F_n is the normal force, μ is the dynamic coefficient of friction, and v_{tr} is the transition velocity. Above the transition velocity this function behaves the same as Coulomb friction. Below the transition velocity this function provides a gradual reduction in the friction force as opposed to the discontinuous behaviour of the Coulomb model. These parameters are left as variables to be optimized later The friction force, F_f, is applied to the ball and clubhead at the point of contact and against the direction of relative motion.

3.2.2 Maw Model Extended for Drivers and Irons

This model developed by Maw *et al* [35], was originally developed for 2D impacts of elastic spheres against a fixed plate. In this section, two changes are made to the Maw model to make it more suitable for predicting golf impacts. First, the original Maw model predicts perfectly elastic collisions as it utilizes Hertzian contact theory. To model inelastic collisions, a Hunt-Crossley damping term is added to the normal force equation. This produces equation 3.16.

$$F_N = kx^{\frac{3}{2}} + dx^{\frac{3}{2}}\dot{x} \tag{3.16}$$

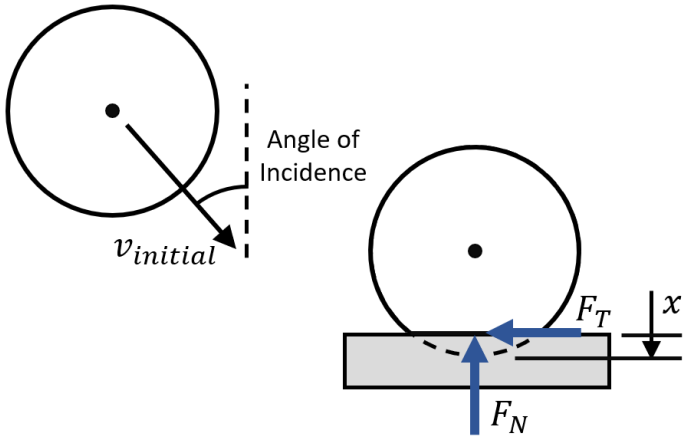

Figure 3.3: Diagram showing the direction of the contact forces for the Maw model.

$$k = \frac{4G\sqrt{R}}{3\left(1-\nu\right)} \tag{3.17}$$

The first term in equation 3.16 is the original Hertzian normal force model. The second term is a hysteretic damping element that is proportional to the normal (approach) velocity. During the compression phase of the collision, $\dot{x}$ is positive which increases the normal force. During the restitution phase, $\dot{x}$ is negative and the normal force is lower. This makes the collision inelastic and produces an asymmetric normal force history consistent with experiments. The stiffness parameter, k, is derived from Hertzian contact theory and is shown in equation 3.17. G is the effective bulk modulus and ν is the effective Poisson's ratio. In Hertz's contact model, if both bodies are deformable, there properties can be lumped in to a combined value. These material properties are left as variables to be optimized later. Therefore, this model accounts for the deformation of the golf ball and clubhead. In equation 3.17, R is the radius of the sphere. For the iron model this is the radius of the ball. For the driver model, the equivalent radius is used to account for the curvature of the clubface. The equivalent radius is calculated using equation 3.18 [55].

$$\frac{1}{r_{eq.}} = \frac{1}{r_{ball}} + \frac{1}{r_{club}} \tag{3.18}$$

In equation 3.18, r_{ball} is the radius of the ball and r_{club} is the radius of the clubface. First, this modified model is used to predict a 2D collision between a golf ball and a rigid

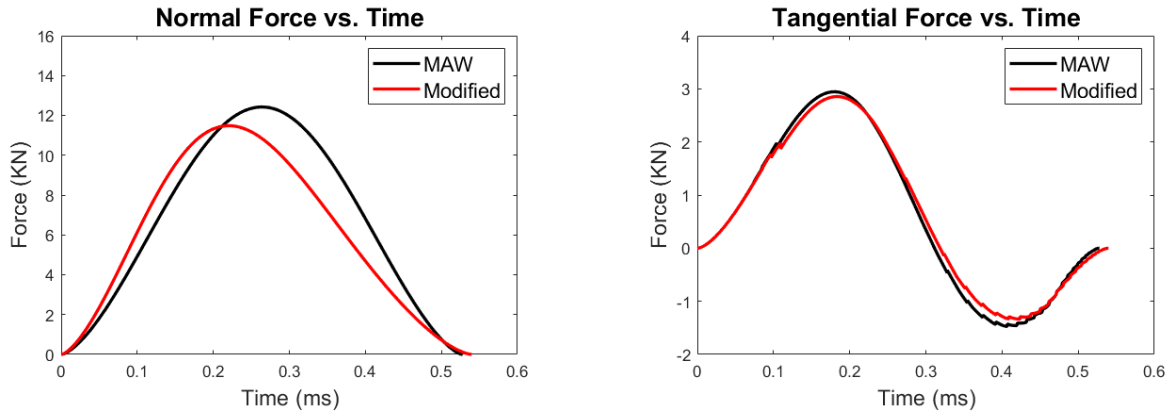

(a) predicted normal forces vs. time.

(b) predicted tangential forces vs. time.

Figure 3.4: Comparison between the original Maw model and the modified model.

plate. Figure 3.3 shows the directions for the normal and tangential forces. These forces are plotted and compared to the original Maw model in figure 3.4. These force histories are for a $44\frac{m}{s}$ impact speed at a 30° angle of incidence.

Figure 3.4a, plots the normal force for the original Maw model and the modified inelastic model. The damping term in equation 3.16 reduces the peak normal force and the area under the curve. The results in the final ball velocity being reduced with the modified model. Additionally, the tangential force histories are slightly different as shown in figure 3.4b. The Maw model calculates the tangential force by dividing the contact area into a series of rings. Here 20 rings are used. These rings can either grip (stick) to the surface or slip. Figure 3.4b, shows this behavoir is slightly different with the new normal force model. Importantly, this modification does not change the tangential force reversal behavior. Inspecting figure 3.4b more closely, reveals they are some discontinuities in the tangential forces. These are caused by the contact area being divide into rings. Using more rings will reduce this behavior. However, the angular velocity plot is much smoother because the integration step acts as a natural filter. While more rings could be used, it has an inappreciable effect on the angular velocity. In conclusion, the addition of damping has the desired effect on the model.

The second change required is due to the original Maw model being derived for 2D collisions. To implement this as a 3D impact model, a 2D normal-tangential frame is assigned as shown in figure 3.5. The origin of this frame is at the point of contact on the

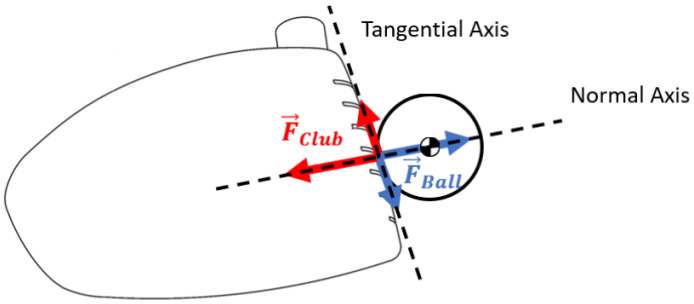

Figure 3.5: Diagram showing the normal and tangential axis reference frame.

clubface. The tangential axis is along the direction of relative motion between the ball and clubhead. The modified normal force is applied along the normal axis. The tangential force is calculated in the same manner as a 2D impact using the relative velocity at the point of contact. Since the ball and clubhead are modeled as free bodies, these contact forces are reversed and applied to the clubhead as well.

3.2.3 Arakawa Model Extended for Drivers and Irons

Arakawa *et al* [13], proposed that tangential force is a function of normal force and the time derivative of the contact area. Once again, this model was originally developed for 2D oblique impacts. Like the Maw model, a normal tangential frame is prescribed at the point of contact. The tangential force model is applied along the tangential axis.

To calculate the time derivative of the contact area, Arakawa used experimental measurements of the contact area. Furthermore, the contact area was used to estimate the normal force throughout the impact. Therefore, to create a predictive impact model that includes tangential forces, an analytical model for the contact area and normal force is required. Hertzian contact theory is used for the normal force and the contact area. Just as in the Maw model, a Hunt-Crossley damping term is added to make the collision inelastic. Therefore, this model is the same in the normal direction as previous modified MAW model. To use the Arakawa tangential force model, the time derivative of contact area is needed. From Hertzian contact theory the contact radius, b, is given by equation 3.19.

$$b = \sqrt{Rx} \tag{3.19}$$

In equation 3.19, R is the radius of the ball and x is the normal normal approach distance. Therefore, the contact area, a, can be expressed as:

$$a = \pi\, b^2 \tag{3.20}$$

$$a = \pi\, Rx \tag{3.21}$$

Taking the time derivative of this equation gives:

$$\frac{da}{dt} = \pi R\dot{x} \tag{3.22}$$

Equation 3.22 shows the time derivative of the contact area is proportional to the normal approach velocity according to Hertzian contact theory. Therefore, the tangential force expression proposed by Arakawa *et al* can be written as:

$$F_T = \mu F_N + \mu\eta\, \pi R\dot{x} \tag{3.23}$$

In equation 3.23, μ and η are contact parameters, however, μ is not a friction coefficient. This equation is used to predict the tangential force. To predict the normal force, Equation 3.16 from section 3.2.2 is used. This includes a damping parameter which makes the collison inelastic.

3.2.4 Experimental Validation

Impact models models are typically validated by measuring and comparing the contact forces during a collision. Several researchers have done with for golf balls impacting a rigid plate [13, 20] Measuring these forces between a golf club and ball during a swing is not practical due to the short impact duration. It would also need to be done in a manner that would not affect the golfer's swing. Instead, to validate these models here, the predicted launch conditions of the ball are compared with the measured launch conditions. These impact models are forward dynamic simulations. Therefore, the more accurate the contact forces, the more accurate the predicted launch conditions should be.

The same set of experimental data used in section 3.1 is used here as well. This data consists of 550 drives and 120 7-iron shots by elite-level golfers. The club properties are the same as listed in table 3.1 Also, the parameter identification method outlined in section

3.1 is used again. The same optimization process and objective function is used for these continuous models.

These continuous impact models are developed in Maplesim, version 2022.1 (Maplesoft, Waterloo, Canada). Maplesim is a multi-domain modeling and simulation software. Here it is used to create multi-body dynamic models of a clubhead and ball. Custom components are made for the contact forces outline in this section. Maplesim produces symbolic equations of motion and numerically differentiates these DAEs. The built-in solvers are used. A fourth order Runge-kutta scheme was used.

3.2.5 Results and Discussion

Table 3.5 summarizes the accuracy of the volumetric contact model outlined in section 3.2.1. Table 3.5 lists the mean absolute error and standard deviation for each launch condition. The relative error is shown as a percentage in parentheses. This is percentage is calculated from the experimental mean which is shown in the left column. Table 3.5 also shows the optimized contact model parameters and average CPU time. This the average time to run one simulation.

From table 3.5, ball speed has the lowest normalized mean absolute error of 2% or less for both models. Launch angle is the next best with normalized errors between 3% to 5%. The predicted backspin is also reasonable with normalized mean absolute errors under 8%. Finally, azimuth (horizontal launch angle) and sidespin have the largest relative errors. From table 3.5, the normalized mean absolute error for these launch conditions is between 30% and 50%. However, the magnitude of these errors is comparable to backspin and vertical launch angle errors. The normalized errors for sidespin and azimuth are larger due to the experimental mean values being relatively smaller.

Interestingly, the ball parameters and friction coefficients are different between the driver and 7-iron models. Comparing the parameters in table 3.5, the coefficient of friction, μ, is higher for the 7-iron model. An iron clubface has grooves that are deeper and spaced closer together compared to a driver clubface. Therefore, this result is reasonable. Also from table 3.5, the ball parameters, k_{Ball}, c_{Ball}, and t_{cover} are greater for the 7-iron model. These parameters are likely tied to the friction coefficient.

Table 3.6 summarizes the accuracy of the modified Maw model for both the driver and 7-iron model. Table 3.6 also shows the optimized model parameters and average CPU

Table 3.5: Mean absolute error, standard deviation and model parameters for the two-layer volumetric contact model.

	Driver		7-Iron	
	MAE	STD	MAE	STD
Speed (mph)	2.12 (1.33%)	2.91 (1.83%)	2.42 (2.06%)	1.65 (1.41%)
Launch (deg)	0.54 (3.72%)	0.55 (4.00%)	0.77 (4.07%)	0.88 (4.66%)
Azimuth (deg)	1.07 (48.8%)	0.52 (23.7%)	0.70 (32.0%)	0.48 (21.9%)
Backspin (rpm)	228 (7.65%)	239 (8.02%)	436 (6.72%)	272 (4.19%)
Sidespin (rpm)	227 (46.3%)	252 (51.4%)	363 (53.3%)	256 (36.6%)
K_v $\left(\frac{N}{m^3}\right)$	6.25×10^9		6.83×10^9	
d $\left(\frac{ms}{m}\right)$	6.42		9.26	
μ	0.372		0.489	
k_{Ball} $\left(\frac{N\ m}{rad}\right)$	13.5		34.1	
c_{Ball} $\left(\frac{ms}{rad}\right)$	2.53		13.2	
$t_{cover}(mm)$	1.26		2.55	
V_{tr} (m/s)	0.936		0.812	
Avg. CPU Time (ms)	69.3		72.1	

time.

Comparing tables 3.5 and 3.6 shows that the predicted launch conditions for the modified Maw model are less accurate than the volumetric model. However, there are two exceptions where the Maw model performed better. Ball speed with the 7-iron model has a slight improvement and launch angle for the driver has another small improvement. Comparing the average CPU time, the modified Maw model takes about two times longer to run. This is expected, as calculating the contact forces with the Maw model is more computationally intense. For each time step in the Maw model, there is an iterative process to determine the stick and slip boundary conditions of each ring. Lastly, comparing the model parameters in table 3.6, the 7-iron model has a higher friction coefficient (μ) and a higher damping coefficient compared to the driver model. This is consistent with the model parameters identified for the volumetric model.

Table 3.7 summarizes the accuracy of the modified Arakawa model for both driver and

Table 3.6: Mean absolute error, standard deviation and model parameters for the modified Maw model.

	Driver		7-Iron	
	MAE	STD	MAE	STD
Speed (mph)	2.27 (1.43%)	3.07 (1.93%)	2.26 (1.93%)	1.61 (1.38%)
Launch (deg)	0.52 (3.72%)	0.59 (4.00%)	1.52 (8.04%)	1.06 (5.61%)
Azimuth (deg)	1.13 (51.6%)	0.52 (23.7%)	0.73 (33.3%)	0.46 (21.0%)
Backspin (rpm)	385 (12.9%)	356 (11.9%)	653 (10.0%)	477 (7.35%)
Sidespin (rpm)	298 (60.8%)	334 (68.1%)	358 (52.6%)	245 (35.9%)
E (GPa)	15.7		16.3	
$d\left(\frac{ms}{m}\right)$	6.50		11.5	
μ	0.360		0.519	
ν	0.407		0.418	
Avg. CPU Time (ms)	146		159	

7-iron models. Table 3.7 also shows the optimized model parameters.

Comparing tables 3.5 and 3.7 reveals the predicted launch conditions using the Arakawa tangential force model have greater error compared to the volumetric model. The largest increases in error are observed for backspin and sidespin. While the Arakawa model demonstrated good experimental agreement for impacts against a fixed plate, it does not perform well here. This is likely to due to model being validated at specific impact speeds and angles of incidence. Using experimental data, the clubhead velocity and delivered loft will vary substantially from player to player, even using the same club.

In conclusion, the volumetric contact model with a two-layer ball is the best of the models considered in this section. This model returned the lowest error cost function for both the 7-iron and driver models. The modified Maw model is the next best. Two of the individual predicted launch conditions had less error compared to the volumetric model. Overall, the volumetric model is the best choice of the continuous models. Lastly, the Arakawa tangential force model performed considerably worse across all launch conditions.

Table 3.7: Mean absolute error, standard deviation and model parameters for the modified Arakawa model.

	Driver		7-Iron	
	MAE	STD	MAE	STD
Speed (mph)	2.29 (1.44%)	3.12 (1.96%)	3.33 (2.85%)	2.17 (1.85%)
Launch (deg)	0.76 (5.24%)	0.86 (5.93%)	1.63 (8.63%)	0.94 (4.97%)
Azimuth (deg)	1.16 (53.0%)	0.54 (24.7%)	0.82 (37.4%)	0.49 (22.4%)
Backspin (rpm)	634 (21.3%)	582 (19.5%)	998 (15.4%)	953 (14.7%)
Sidespin (rpm)	316 (64.4%)	348 (71.0%)	403 (59.2%)	297 (43.6%)
E (GPa)	15.1		14.6	
$d\left(\frac{ms}{m}\right)$	6.35		9.89	
μ	0.0486		0.118	
η	1.32×10^5		2.06×10^5	
Avg. CPU Time ms	58.6		63.5	

3.2.6 Comparison Between Discrete and Continuous Models

The purpose of this section is to compare the results between the continuous impact models and the discrete models. First, the results for the driver models are examined. From section 3.1.4, the best discrete driver model is the adjusted IM model proposed by Danaei *et al* From section 3.2.5, the two-layer ball with a volumetric normal force model was selected from the proposed continuous models. Both models are validated with the same set of experimental data. Therefore, the mean absolute errors can be compared directly. Comparing tables 3.3 and 3.5 reveals that the adjusted IM model is overall the most accurate. The volumetric model performed slightly better for predicted launch angle. The remaining launch conditions are all in favour of the adjusted IM model. However, the model accuracy is not the only consideration for selecting an impact model. The computational efficiency is important depending on the use case. The adjusted IM model required two orders of magnitude less time to run compared to the continuous models. This is expected, as the continuous models need to calculate hundreds of positions and velocities throughout the impact. In conclusion, for predicting the launch conditions of a drive, the adjusted IM model seems to be the best choice of the models considered.

For the 7-iron, the adjusted IM model and volumetric models are also the most accurate. Comparing tables 3.3 and 3.5 shows that both models have strengths. Mean ball speed and sidespin errors are slightly improved with the adjusted IM model. The volumetric model leads the other launch conditions with a significant 132 rpm reduction in mean backspin error. Equation 3.13 is the cost function used to tune each models parameters. During this process, the IM model returned a cost function value of 1.05 and the volumetric model returned a value of 0.98. Therefore, only considering accuracy, the volumetric model is the best for predicting a 7-iron shot. Comparing the average CPU times shows the IM model requires two orders of magnitude less time to run. However, the continuous model can still run in under 0.1 seconds, which is likely sufficient for most use cases. In conclusion, for predicting the launch conditions of a 7-iron, the two-layer ball with a volumetric normal force model is the preferred choice although IM models are still a useful tool if the faster compute time is needed.

Chapter 4

Golf Club and Ground Modeling

The purpose of this section is to model the ground reaction forces experienced by the clubhead. During a drive, the ball is hit off a tee that elevates it off the ground. Typically, the tee height is about 2 inches, while a maximum height of 4 inches is set by the USGA [10]. During a drive, the clubhead should never touch the ground and doing so results in poor shot. Therefore, modeling the driver is not considered in this chapter. During an iron shot the ball is usually resting on the turf. An elite golfer will strike the ball with the clubhead just above the ground. After impact the club strikes the ground, creating a divot. This allows the golfer to hit downwards, improving the launch conditions. In figure 4.1 this type of strike is labeled as 'good'. Figure 4.1 also shows the common types of mishits for iron shots.

If the ball strike is low on the clubface, the shot is referred to as 'thin'. This will affect ball flight and distance. If the ball strikes the leading edge of the club, the shot is referred to as 'bladed' or 'topped'. This results in a significant distance loss and a low trajectory. The iron model constructed in chapter 3 is valid for 'thin' shots but not 'topped' or 'bladed' shots. When the ball strikes higher on the clubface, the shot is referred to as 'fat'. When this happens the clubhead hits the ground before the ball. As illustrated in figure 4.1, the clubface is in contact with the ground during impact. The iron model in chapter 3 is not valid for this type of mishit as the ground reaction forces were not modeled.

In 2022, Corke *et al* recorded 1127 5-iron shots with golfers of varying abilities and measured clubhead kinematics at impact [56]. Across all participants, 31.7% of shots were labeled as fat. On the other hand, just 2.2% of shots were either 'topped' or hit off the

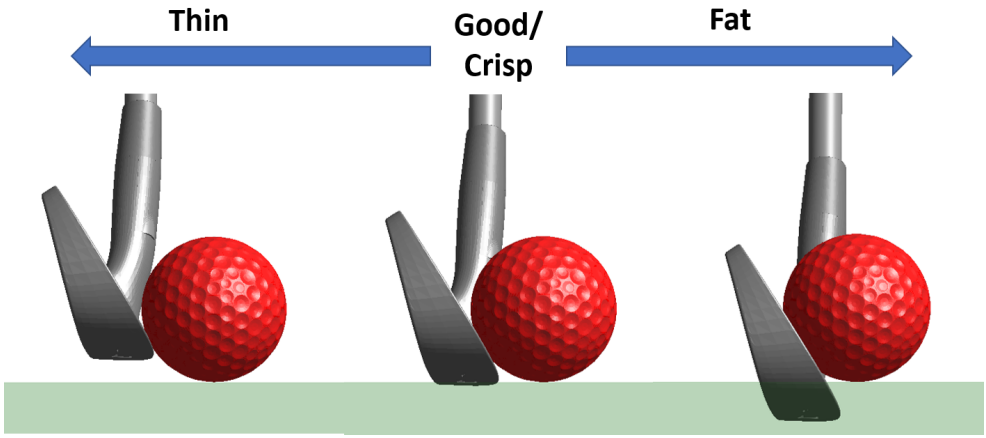

Figure 4.1: Diagram of iron strike classification.

hosel, while the remaining shots were labeled as good or thin. Therefore, extending the iron model to predict fat shots will cover the majority of swings. This model can be used to examine the change in launch conditions for fat shots and how club properties affect performance. For this purpose, a forgiving design is one that minimizes the difference in launch conditions between a fat and a good strike.

4.1 Shaft Model

The impact models in chapter 3 neglected the shaft due to the short duration of the impact. When a golfer makes a divot, the contact time with the ground is significantly longer. Furthermore, the shaft may influence the face angle as the club digs into the ground. This would influence the predicted launch conditions of a fat strike. Therefore, the free-body assumption used earlier can not be applied to this scenario. The purpose of this section is to explain the process of adding a flexible shaft model to the impact model from chapter 3. The two-layer ball volumetric contact model is used as it was the most accurate of the iron models.

In the last decade, the golf equipment market has been flooded with hundreds of different shaft models. The two main parameters that determine a shaft's performance are the material and shape profile. Shafts are typically constructed of steel alloys, graphite, or composite materials. The 7-iron modeled in chapter 3 used a steel shaft. All golf shafts

follow a tapered profile. The largest diameter of the shaft is where the golfer grips the club and is referred to as the butt end. The opposite end of the shaft has the smallest diameter and is referred to as the tip. Manufacturers vary the diameter and wall thickness along the length of the shaft to change the bending properties. As per the equipment regulations, the shaft must be symmetric along its length [10]. Therefore, the radius or thickness can not change around the circumference. Table 4.1 shows the dimensions and mass of the 7-iron shaft.

Table 4.1: Properties of the 7-iron shaft.

Parameter	Value
Mass (g)	104
Length (m)	0.965
Butt radius (mm)	7.6
Tip radius (mm)	4.7
E-Young's Modulus (GPa)	190 (SAE 8655 Steel)
ν-Poisson's Ratio	0.29 (SAE 8655 Steel)

The golf industry has widely adopted a three-point bending test to measure a shaft's stiffness. The shaft is supported at two points and a load is applied at the center as illustrated in figure 4.2. There are two properties that affect the bending behavior of a shaft: the Young's modulus (E) and second moment of area (I). In solid mechanics, this behavior is governed by equation 4.1. The golf industry frequently lumps Young's modulus and second moment of area together, simply referred to as EI. To characterize shaft stiffness, the three-point bending test is performed at several locations along the length of the shaft. This produces a plot referred to as an EI curve.

$$\delta_x = \frac{FL^3}{48EI} \tag{4.1}$$

Figure 4.3 shows the measured EI curve of the 7-iron shaft. To model the shaft, a series of hollow tapered cylinders is used. The goal is to produce a simplified model with a similar bending stiffness along the shaft's length. The Young's modulus of the shaft material is 190 GPa. Steel shafts are typically manufactured using rolling and welding processes. After

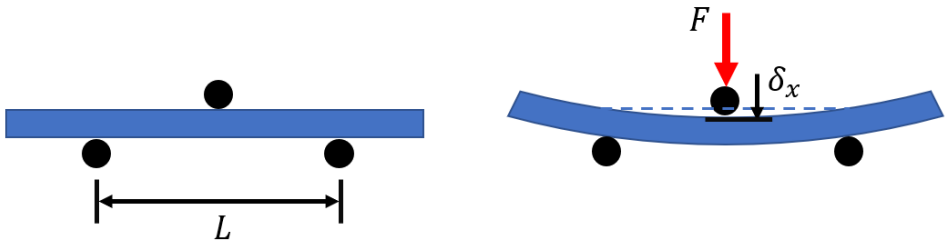

Figure 4.2: Schematic of 3-point bending test.

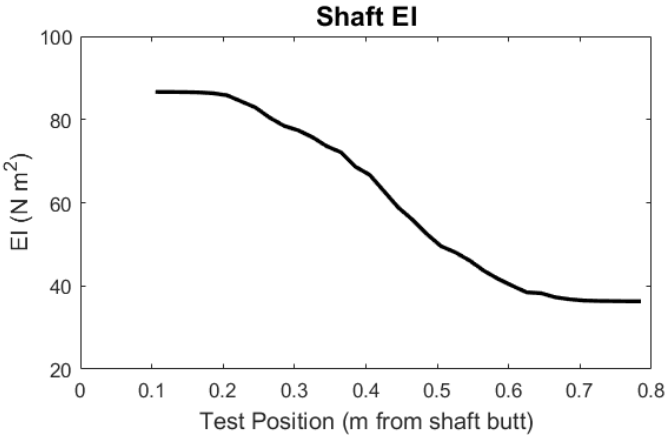

Figure 4.3: 7-iron shaft EI measurements.

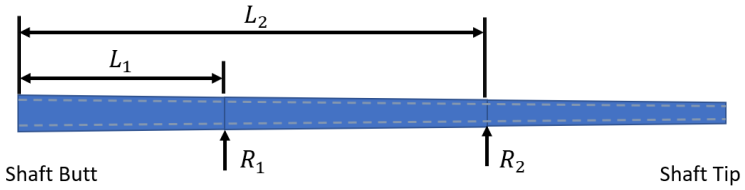

Figure 4.4: Shaft dimensions.

these processes, they are typically heat treated to remove residual stresses. Therefore, the shaft model will assume the material is isotropic. The bending stiffness is now only dependent on the second moment of area. Three sections are used in the model as the measured EI curve follows an "s" shape. The radii at the tip and butt end are set to the values in table 4.1. The other dimensions, shown in figure 4.4, are determined using an optimization process. These dimensions are optimized to minimize the difference between the measured EI curve and model EI. The method of least squares is used to determine the best fit. These shaft dimensions are shown in table 4.2.

Table 4.2: Optimized dimensions for the model shaft.

Shaft Dimension	Value
Wall Thickness - Butt (mm)	0.348
Length 1 - L_1 (m)	0.273
Radius 1 - R_1 (mm)	7.24
Wall Thickness 1 (mm)	0.381
Length 2 - L_2 (m)	0.609
Radius 2 - R_2 (mm)	5.08
Wall Thickness 2 (mm)	0.549

Figure 4.5 compares the experimental and model EI curves. The three-segment model does a sufficient job of capturing the change in stiffness. Adding more sections would have a marginal improvement at a higher computational cost. From these dimensions, the volume of the shaft can be calculated. Using a density of $7.46 g/cm^3$, the model shaft mass is 104g. With these material properties and dimensions, the model shaft has the same

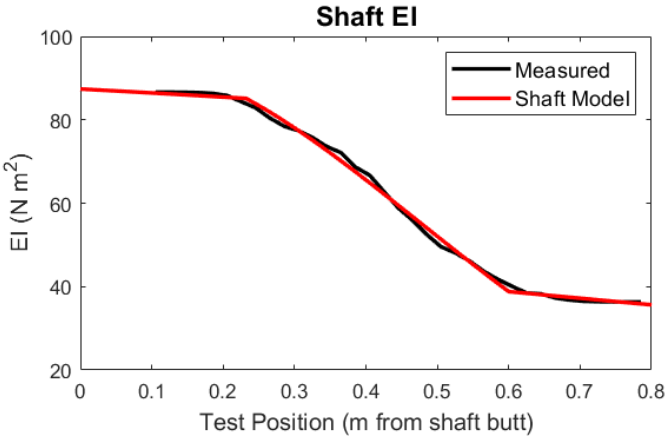

Figure 4.5: 7-iron shaft EI measurements

mass and similar deflection properties. The other important property that affects a golf shaft's performance is the torsional stiffness. The angle of twist is governed by equation 4.2.

$$\theta = \frac{TL}{GJ} \tag{4.2}$$

The torsional stiffness is influenced by the shear modulus, G, and geometry of the shaft. In equation 4.2, T is the applied torque, L is the length of the shaft, and J is the second moment of area. While the material composition is known, the torsional behavior of the shaft was not measured. It is assumed using the shaft geometry described above and the shear modulus of the shaft will provide a reasonable estimate. To implement this into the multibody dynamics model from chapter 3 requires some constraints. The position and orientation of the grip end is kinematically driven. To interpolate between the motion capture data, a constant acceleration between points is assumed. The shaft model is allowed to deflect, twist, and elongate during the simulation. There are no experimental measurements of a golf shaft elongating during a swing. However, this model defines the position of the clubhead and grip end of the shaft. Therefore, not allowing the shaft to elongate would over constrain the system. Figure 4.6 shows the full club model in Maplesim, including the clubhead and grip coordinate frames.

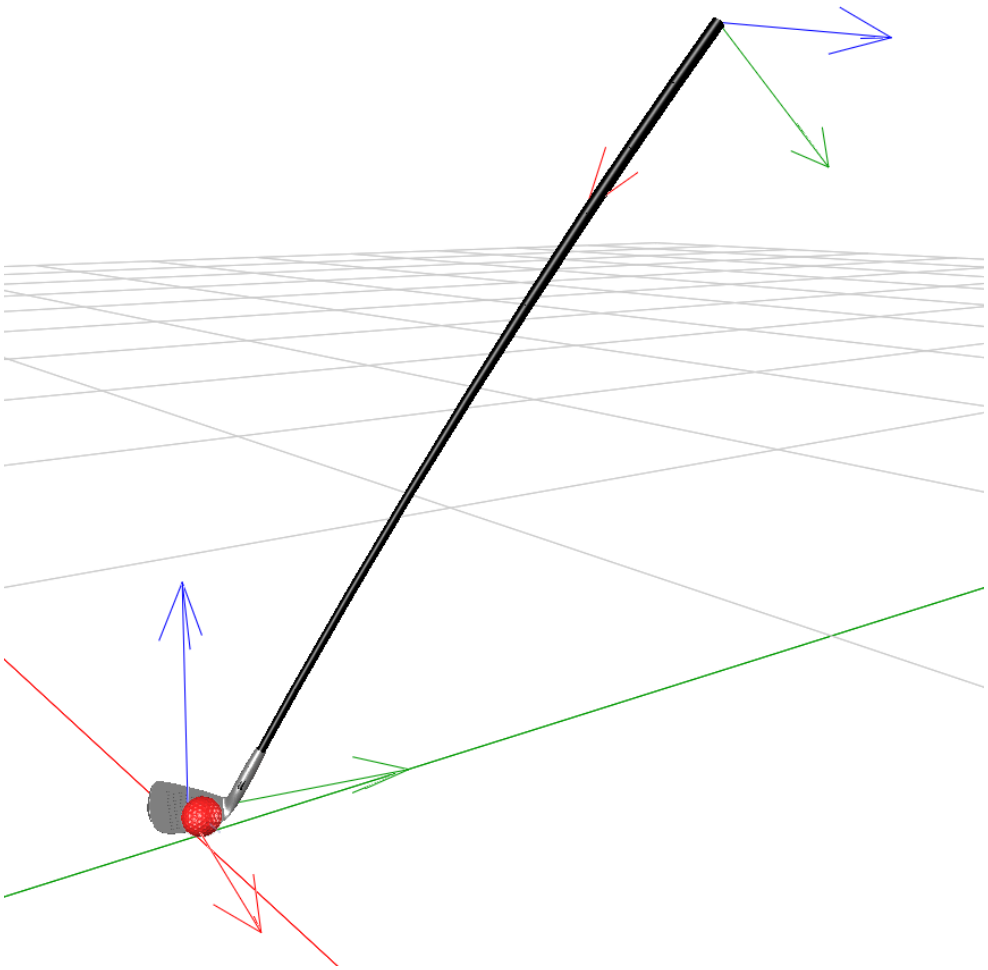

Figure 4.6: 7-iron model with flexible shaft in Maplesim.

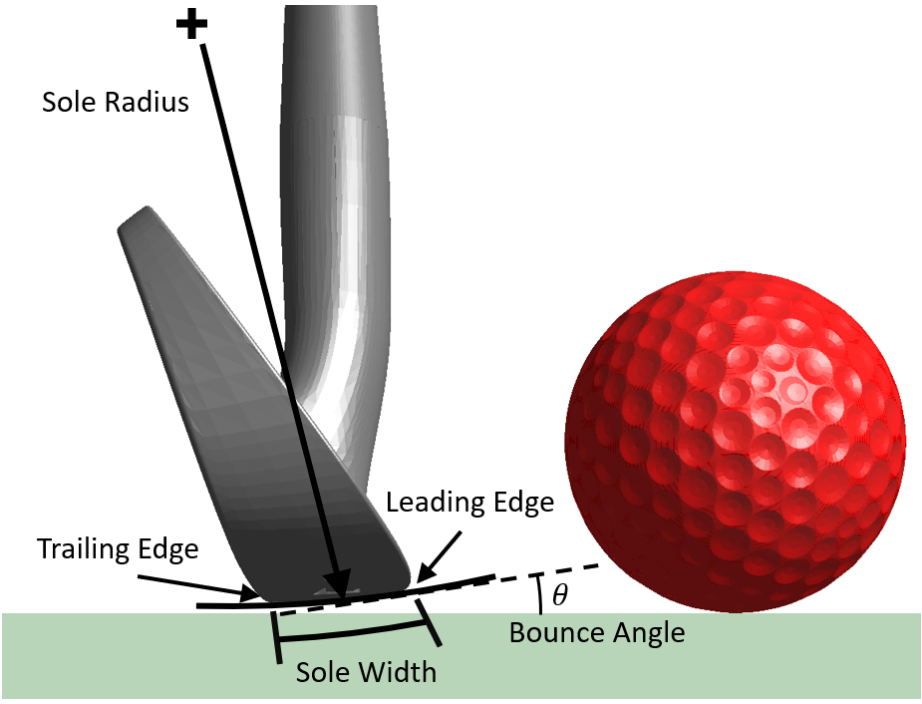

Figure 4.7: Diagram of a typical iron sole.

4.2 Clubhead-Ground Model

The lowest portion of the clubhead is referred to as the sole and is typically the first part of the club to hit the ground. Golf equipment manufactures spend a large amount of time designing the sole of irons and wedges. The shape of this surface plays a major role in the feel and forgiveness level of a club. The industry commonly refers to this geometry as the sole grind. Equipment manufactures offer several different grinds. However, little is understood about the effect on performance. The purpose of this section is to develop a parameterized model for the sole of an iron and wedge.

There are hundreds off different sole designs on the market. Figure 4.7 shows the main design characteristics for most irons. The sole width is the distance from the leading edge to the trailing edge. The bounce angle is measured from the ground to the tangent line of the club sole at the leading edge as shown in figure 4.7. Finally, the sole radius measures the amount of curvature. To approximate this geometry, a cylindrical section is used. The radius of the cylinder is the sole radius. The segment spans from the leading to trailing

edge of the club. The cylinder length is the width of the clubhead. The following sections use this geometry to model the contact forces.

For modeling purposes, the contact between the clubhead and ground is divided into two phases. Typically, during the downswing, typically the sole is the first part of the club to make contact with the ground. During this first phase the leading edge is above the playing surface and the trailing edge is below the playing surface. In this chapter, this is referred to as the compression phase. Here the ground is displaced vertically but not horizontally. The second phase begins when the leading edge is below the playing surface. When this occurs, the clubface is in contact with the ground. This is the phase that creates the divot as the ground is being displaced horizontally. It is important to distinguish between these phases in the following sections for modeling.

4.2.1 Club Sole Model

This section focuses on the forces experienced by the sole of the clubhead. The term turf generally describes the top layer of grass and soil down to the roots. For modeling purposes, the grass is not considered here. This model only considers the contact forces caused by the soil. Therefore, this model is most applicable to hitting from a fairway. These areas of a golf course consist of short thin grass. To estimate the ground reaction forces (GRFs), models from the field of terramechanics (study of terrain behavior for off-road vehicles) are applied.

From the field of terramechanics, the force-depth relationship is well documented and measured for a variety of soils. For the golf model, Bekker's empirical pressure-sinkage model is used [57]. While there are dozens of other models for this behavior, Bekker's model has been used for decades and there are several experimentally-measured soil parameters in the literature.

$$\sigma\left(z\right) = \left(\frac{k_C}{b} + k_\varphi\right) z^n \tag{4.3}$$

Equation 4.3 is Bekker's emperical pressure sinkage relation, where k_C, k_φ, and n are soil parameters. b is the smaller dimension of the contact area. Bekker developed a simple wheel-soil model to predict contact forces during locomotion [58]. This model assumes the tyre is perfectly rigid with a smooth outer surface. Other researchers have developed newer models for pneumatic wheels and tyre lugs. These models and discrete element models have

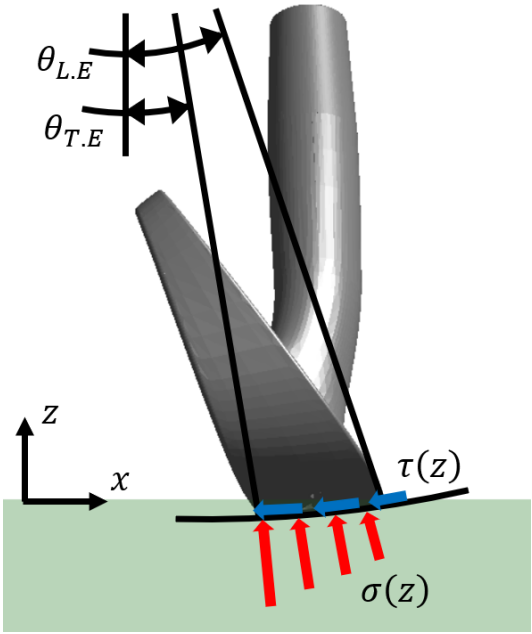

Figure 4.8: Diagram of the ground reaction forces acting on the club sole.

replaced Bekker's rigid wheel model in this field. However, for the purpose of modeling the sole of a golf club, Bekker's assumptions are valid as the clubhead is typically polished steel. The club sole model developed in this section is derived similarly to Bekker's rigid wheel model. Figure 4.8 shows the ground reaction forces applied to the club sole.

In figure 4.8, σ is the soil pressure calculated from Bekker's pressure sinkage relation. The total sinkage force is determined by integrating this pressure over the club sole. The resulting force is applied perpendicular to the sole radius. To perform this integration, a cylindrical reference frame is used. This reference frame coincides with the cylinder that approximates the sole radius. The leading edge angle, $\theta_{L.E}$, describes the position of the leading edge in the cylindrical reference frame. Similarly, the trailing edge angle, $\theta_{T.E}$, is the position of the trailing edge. This gives the following expressions for the horizontal and vertical forces acting on the clubface.

$$F\sigma_x = -w \int_{\theta_{T.E}}^{\theta_{L.E}} \sigma(z)\ r_{sole} \sin(\theta)\ d\theta \tag{4.4}$$

$$F\sigma_z = w \int_{\theta_{T.E}}^{\theta_{L.E}} \sigma(z)\ r_{sole} \cos(\theta)\ d\theta \tag{4.5}$$

Equation 4.4 is the horizontal force and equation 4.5 is the vertical force due to soil compaction. These forces are applied at the centroid of the distributed force. In these equations, w is the length of the cylindrical section (this is the width of the club sole). From figure 4.8, the horizontal component is to the left, thus the negative sign in equation 4.4.

To predict the shear force along the club sole, the relative motion is considered. In the field of terramechanics, this is referred to as the skid of a wheel. For a wheel locked under braking, the skid is 100%. This best describes the club sole being pushed through the ground. Therefore, the shear stress on this surface is assumed to be the shear strength of the ground. The shear strength of soils and other terrain types is commonly modeled using the Mohr-Coulomb failure criterion [50], shown in equation 4.6.

$$\tau_{max} = \ c \ + \ \sigma \tan \Phi \tag{4.6}$$

In equation 4.6, c is a soil parameter relating to the cohesion between particles. For dry sand and soils, this parameter is often ignored. σ is the normal stress experienced by the soil. Φ is another soil parameter referred to as the angle of internal shearing resistance. For most soils, this parameter is around 30°. However, $\tan(30°)$ is exactly $\frac{1}{\sqrt{3}}$, which is the relation proposed by the Von Mises yield criterion. Therefore, equation 4.7 is used to determine the shear strength.

$$\tau_{max} = \ \frac{\sigma(z)}{\sqrt{3}} \tag{4.7}$$

The total shear force is calculated by integrating this stress across the club sole. This force is applied along the tangent of the sole radius. Equations 4.8 and 4.9 are the horizontal and vertical components of this shear force.

$$F\tau_x = -w \int_{\theta_{T.E}}^{\theta_{L.E}} \frac{\sigma(z)}{\sqrt{3}} \, r_{sole} \cos(\theta) \ d\theta \tag{4.8}$$

$$F\tau_z = -w \int_{\theta_{T.E}}^{\theta_{L.E}} \frac{\sigma(z)}{\sqrt{3}} \, r_{sole} \sin(\theta) \ d\theta \tag{4.9}$$

The forces defined by equations 4.4, 4.5, 4.8, and 4.9 are applied when any portion of the club sole is in contact with the ground. Therefore, these forces apply to both phases of the ground contact. The normal stress in all of these equations is a function of depth. This needs to be considered during integration.

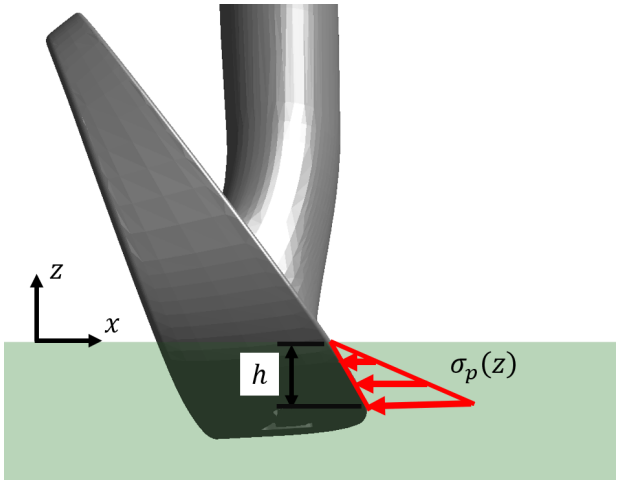

Figure 4.9: Diagram of the ground reaction forces acting on the clubface.

4.2.2 Clubface Model

This section focuses on the GRFs experienced by the clubface. These forces are applied when the leading edge of the club is below the playing surface. Here this is defined as the second phase of the contact with the ground. The clubface is the surface that horizontally displaces the ground, creating a divot. Hence, the reaction force is calculated in the same manner as earth moving equipment. Figure 4.9 shows the reaction forces applied to the clubface.

In Figure 4.9, σ_p is referred to as the passive earth pressure in the field of terramechanics. This is the pressure exerted by the soil in the horizontal direction, which increases with soil depth. Equation 4.10 is commonly used to model this relation [50].

$$\sigma_p = \gamma_s z N_\Phi + 2c\sqrt{N_\Phi} \tag{4.10}$$

The first term in equation 4.10 corresponds to the weight of the soil, where γ_s is the density of the soil and z is the depth. In the second term of this equation, c is the cohesion of the soil. Once again, the cohesion behavior is ignored, as it assumed the ground consists of dry sand and soil. Therefore, only the first term of equation 4.10 is considered. N_Φ is referred to as the flow value and is a dimensionless quantity. This is related to the angle

of internal shearing resistance by equation 4.11.

$$N_\Phi = \tan^2\left(45^\circ + \frac{\Phi}{2}\right) \tag{4.11}$$

Once again, the internal shearing resistance is assumed to be 30°. Solving equation 4.11, gives a flow value of 3. Typically, these types of earth moving models include a force parallel to the cutting surface. This is caused by the shear force as material moves relative to the cutting surface. This force is highly experimental and depend on a variety of factors such as the angle of the blade and surface roughness. Here the forces parallel to the clubface are ignored for simplicity. Therefore, to calculate the force acting on the clubface, only the soils passive pressure is considered. The net force is calculated by integrating pressure across the clubface. This gives equation 4.12.

$$F_P = \int_0^h w\ \sigma_P\ dz \tag{4.12}$$

$$F_P = w\ \left(\frac{1}{2}\gamma_s N_\Phi h^2\right) \tag{4.13}$$

In equation 4.12, w is the width of the clubhead and h is the depth of the leading edge. Substituting in the equation for σ_P and performing the integration gives equation 4.13. This is the horizontal component of the force required to push the clubface through the soil. This force is applied at the centroid of the applied force distribution. From figure 4.9, this point is at a depth of $\frac{2}{3}h$.

4.3 Results

To develop this model, once again Maplesim version 2022.1 (Maplesoft, Waterloo, Canada), is utilized. The two-layer ball volumetric contact 7-iron model from chapter 3 is the starting point. This model was found to be the most accurate of the models considered for predicting iron shots. The soil parameters are estimated using values from literature and considering the construction of a golf course. The purpose of this section is to examine the effect of adding GRFs by comparing the predicted ball launch conditions with and without GRFs.

There are no published experimental pressure-sinkage or shear tests for golf course grounds. There are several published parameters for a variety of soil types, surfaces, and

geographical regions. The fairway and teeing area of a golf course is typically comprised of a mixture of loam and sand. Some fairways are rolled to make the course firmer. Even fairways that are not rolled should have some level of compaction as players, carts, and vehicles traverse them during regular use. This model is used to simulate a soft, medium, and high compaction scenario for a sand-loam composition. The soil parameters for the three scenarios are shown in table 4.3. These values are chosen to represent the range of soil properties in table 2.1. However, soil parameters will vary with different climates and weather conditions.

Table 4.3: Typical properties for soft, medium, and firmly compacted sandy-loam [50].

Parameter	Soft	Medium	Firm
ρ - Density $\left(\frac{g}{cm^3}\right)$	1.53	1.91	2.30
n - Sinkage exponent	0.66	1.00	1.20
$k_c \left(\frac{kN}{m^{n+1}}\right)$	10.5	32.8	48.4
$k_\theta \left(\frac{kN}{m^{n+2}}\right)$	1260	4580	15000

Figure 4.10 shows the predicted contact forces for the soft, medium, and firm soil conditions. Figures 4.10a and 4.10b show the GRFs for a fat shot. The shaded region of these plots is when the ball and clubhead are in contact. These shots are fat because the clubhead strikes the ground before the ball. Therefore the GRFs to the left of this shaped region can influence the launch conditions of the ball. Figures 4.10c and 4.10d show the GRFs during a good shot. Here the clubhead still strikes the ground and ball at the same time. This still creates a divot, however, the GRFs are substantially lower. The vertical line on these plots is when the second contact phase begins. This is when the leading edge is below the playing surface.

Figure 4.10 shows the duration of ball contact is roughly one order of magnitude less compared to the ground contact. As expected, the predicted forces are the highest for the firm condition. Furthermore, across all soil conditions the predicted vertical forces are greater than the horizontal forces. Additionally, all the curves have a similar bell curve shape. The primary difference is magnitude and duration of the contact. Unfortunately, there is no experimental data to compare these contact forces. The interest behind modeling these forces is to see how they influence the launch conditions of the ball.

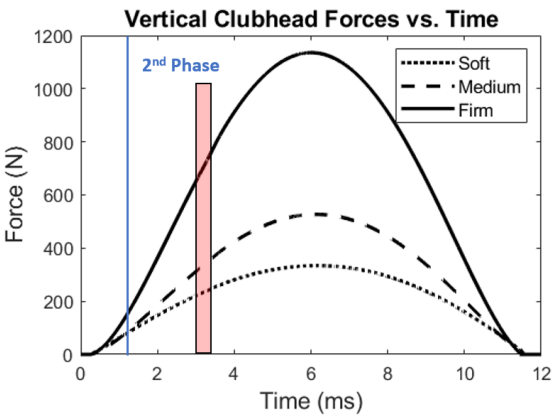

(a) Vertical GRFs during a fat strike.

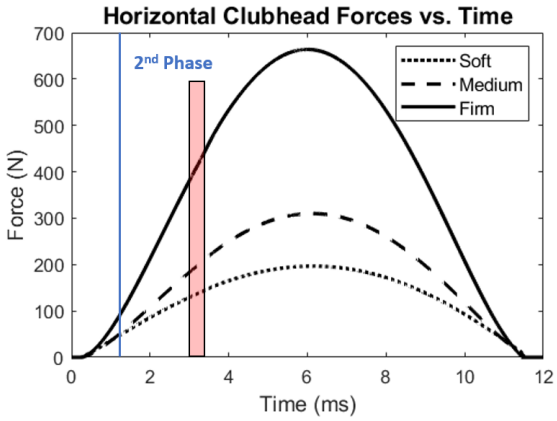

(b) Horizontal GRFs during a fat strike

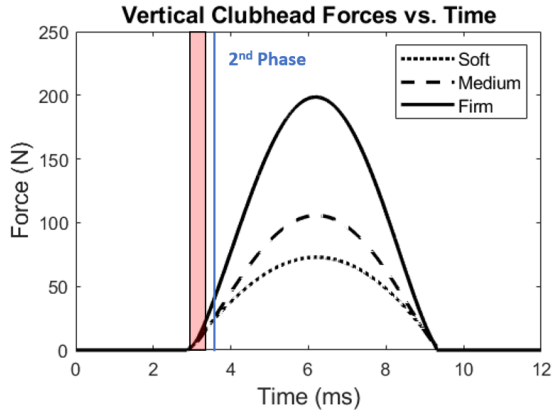

(c) Vertical GRFs during a good strike.

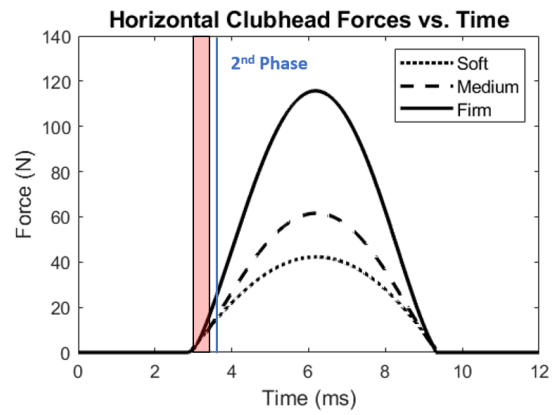

(d) Horizontal GRFs during a good strike.

Figure 4.10: Total GRFs predicted by the model for fat and good strikes.

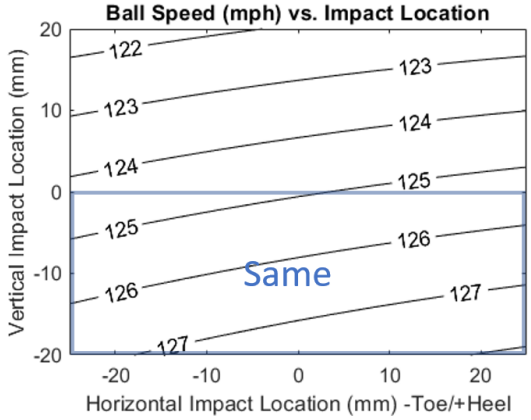

(a) Ball speed without GRFs.

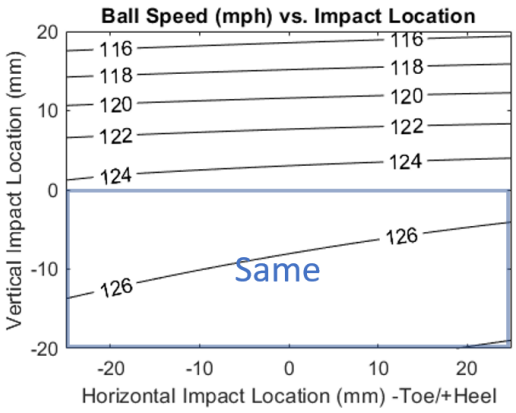

(b) Ball speed with GRFs.

Figure 4.11: Predicted ball speed of the 7-iron models.

To study the effects of the ground reaction forces, the firm soil condition is used. This will produce the largest differences in clubhead velocity compared to a teed ball, and subsequently the predicted launch conditions of the ball. Figure 4.11 compares the predicted ball speed across the clubface simulated with and without ground reaction forces. To produce these plots, the same swing kinematics were used for all shots. The X-axis corresponds to mishits horizontally along the clubface. As shown in figure 4.12, this is referred to as the heel-toe direction. The Y-axis corresponds the vertical impact location. These different impact locations were simulated by changing the ball's position and ground height.

Figure 4.11a is the predicted ball speed without ground reaction forces simulated. The maximum ball speed occurs below the center of the clubface and towards the heel. This makes sense as the clubhead has a low center of gravity and this model includes a flexible shaft. This is consistent with the observations of Dewhurst and McNally *et al* [22, 41]. Comparing the results between the two plots in figure 4.11 shows ball speed is the same for strikes below the center line of the clubface. Here, the clubhead impacts the ball before contacting the ground. These strikes are referred to as crisp or thin. Strikes above the center of the clubface are referred to as 'fat'. For these strikes, the ground reaction forces have an impact on the launch conditions of the ball. Both plots in figure 4.11 show ball speed decreases for shots higher on the clubface. Figure 4.11a shows a 5 mph decrease for high strikes while figure 4.11b shows a 10 mph decrease for similar strikes. Therefore,

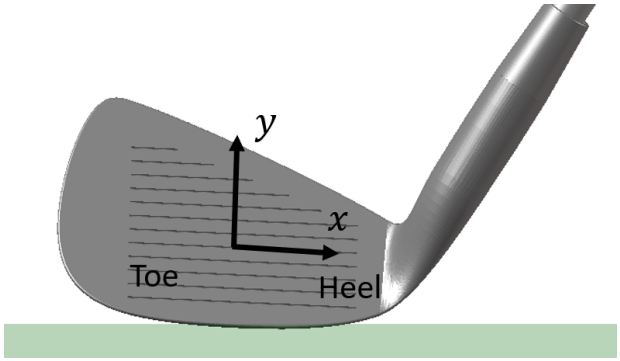

Figure 4.12: Club face axis to specify impact location.

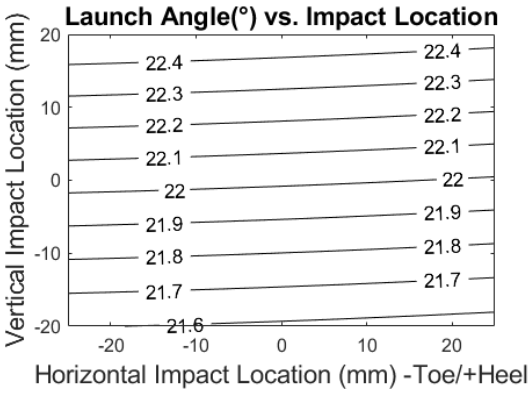

(a) Launch angle without GRFs.

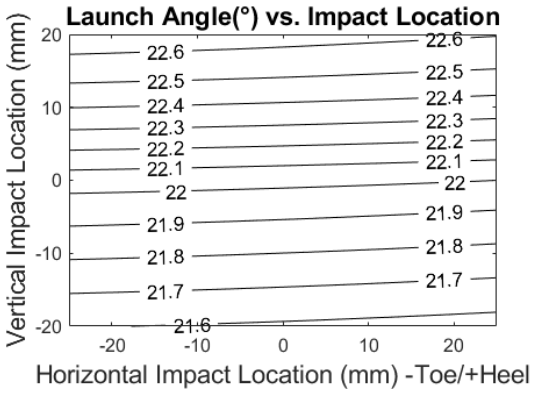

(b) Launch angle with GRFs.

Figure 4.13: Predicted vertical launch angle of the 7-iron models.

including the ground reaction forces results in a further decrease in ball speed for fat strikes.

Figure 4.13 compares the predicted vertical launch angle between these models. Examining figure 4.13a shows that the launch angle increases as the impact location moves up the face. Figure 4.13b shows the same trend is present when the ground reaction forces are modeled. While the launch angles are slightly higher with the ground reaction force model, this behavior is relatively insignificant.

Figure 4.14 compares the backspin and sidespin between these models. Figure 4.14a is the predicted backspin for the iron model without ground reaction forces. The highest backspin is 6140 rpm and occurs along the bottom of the clubface. Backspin gradually

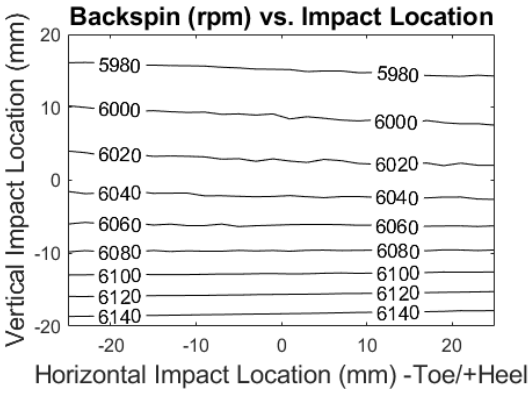

(a) Backspin without GRFs.

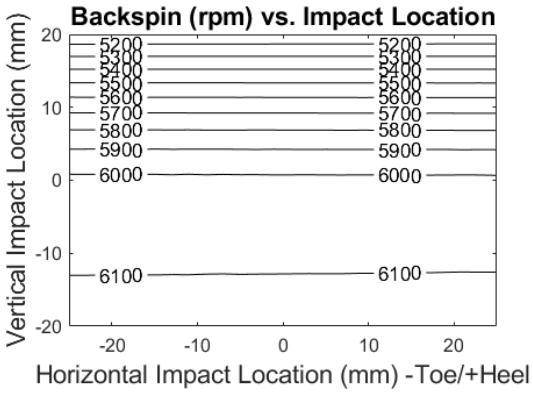

(b) Backspin with GRFs.

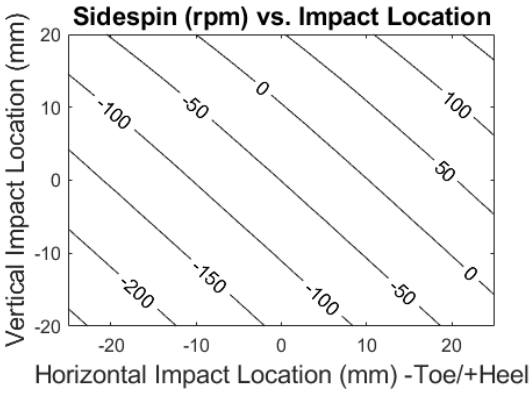

(c) Sidespin without GRFs.

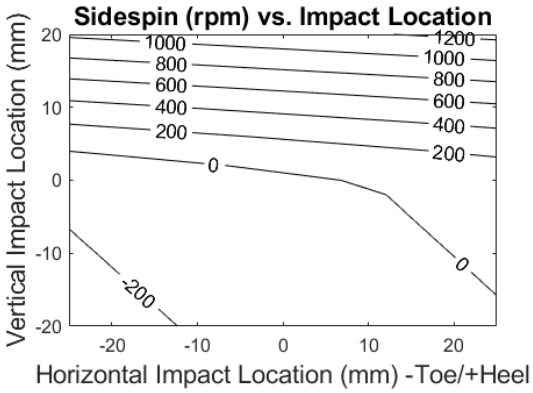

(d) Sidespin with GRFs.

Figure 4.14: Predicted backspin and sidespin of the 7-iron models.

decreases moving up the clubface. Comparing this to the plot with ground reaction forces (figure 4.11b) there is a much greater decrease in backspin. The greatest differences occur along the top of the clubface, which is up to 700 rpm less for the ground model. Plots 4.14c and 4.14d show the predicted sidespin of these models. Without ground reaction forces, sidespin gradually decreases (higher draw spin) as the strike location moves towards the toe of the clubface. Including the ground reaction forces gives a very different result. Figure 4.14d shows fat shots dramatically increase sidespin (higher fade spin). At the top of the clubface, the difference in sidespin is about 1000 rpm. Therefore, the ground reaction forces have a significant influence on the predicted spin.

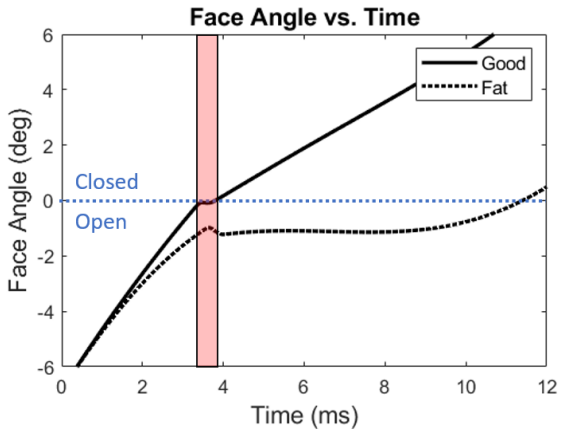

(a) Clubface angle measured about the vertical axis.

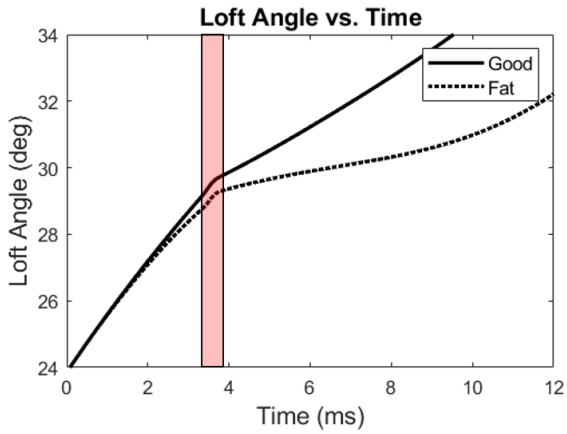

(b) delivered loft (angle between the clubface and vertical axis).

Figure 4.15: Clubface angle and loft during a good and fat strike.

To investigate why the predicted spin is so dramatically different, the clubface orientation is plotted in figure 4.15. The left plot shows the clubface rotation angle measured about the vertical axis. An angle of zero is referred to as a squared clubface. This means the clubface is aligned with the target. The shaded region of this plots is when the ball and clubhead are in contact. Examining figure 4.15a, for the good strike, the clubface is initially open and rotating to become squared at the moment of impact. After impact the clubface continues rotating during the follow through. The fat strike starts similarly, but the clubface is open at the moment of impact due to the GRFs. This produces the high amount of draw spin observed for fat shots. Even after impact, the GRFs reduce this rotation compared to a good strike. Figure 4.15b shows the delivered loft of the clubhead between these two swings. This plot shows that the GRFs are slightly de-lofting the clubface before impact.

It is clear that the GRFs affect the launch conditions of the ball. To gain a more meaningful understanding of this effect, a ball flight model is used to estimate the flight of these shots. In 2022, Ferguson *et al* published an updated golf ball aerodynamic model validated with modern golf balls [59]. The authors recorded over one thousand shots with various types of clubs. The model's parameters are optimized to minimize the error between the measured and predicted distance, offline landing position, and apex. The new fitted model demonstrated a mean absolute error of less than 3 yards (1.52%) for

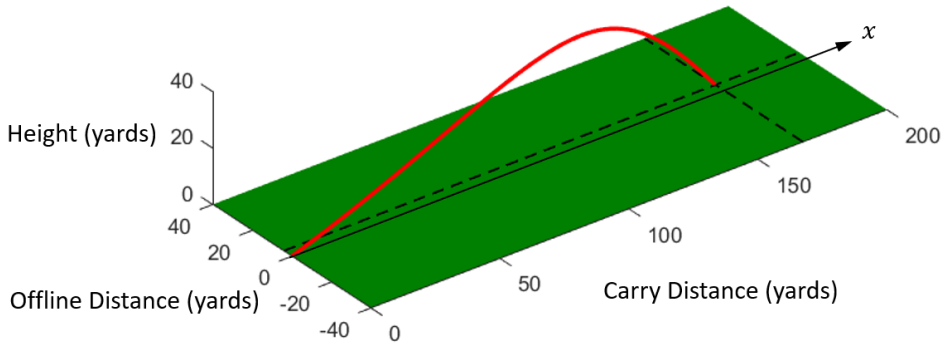

Figure 4.16: Simulated ball trajectory using an aerodynamic model.

carry distance. Figure 4.16 shows one of the simulated ball flights for the 7-iron model. The carry distance is the X-coordinate of the final position and the offline distance is the Y-coordinate. Figure 4.17 compares the ball flight metrics of the 7-iron model with and without the ground reaction forces modeled.

Figures 4.17a and 4.17b compare the carry distances of the 7-iron model with and without ground reaction forces. Both plots show that the maximum carry distance occurs slightly below the center of the clubface and towards the heel. Figure 4.17a shows that the carry distance can decrease up to 7 yards for a strike at the top of the clubface. Comparing this to figure 4.17b, including the ground reaction forces further penalizes off-centre strikes. This model predicts the carry distance for fat shots can decrease up to 12 yards.

Figures 4.17c and 4.17d compare the offline distance between these models. Without ground reaction forces, the offline distance only varies by a few yards left or right. Comparing this to figure 4.17d shows a dramatically different behavior for fat strikes. For strikes above the center of the clubface, the tendency is for the ball to miss right of the target line. This is caused by the sidespin imparted for fat strikes shown in figure 4.14d. This is due to the ground reaction forces rotating the clubface away from the target line as shown in figure 4.15a. This behaviour worsens as the impact location moves up the clubface. At the top of the clubface, the ball can land over 15 yards right of the target line. Therefore, including GRFs has a significant effect on the predicted ball flight for fat strikes.

Validating this ground reaction force model presents challenges. Measuring the soil properties of golf courses can vary due to weather and location. Alternatively, the ground

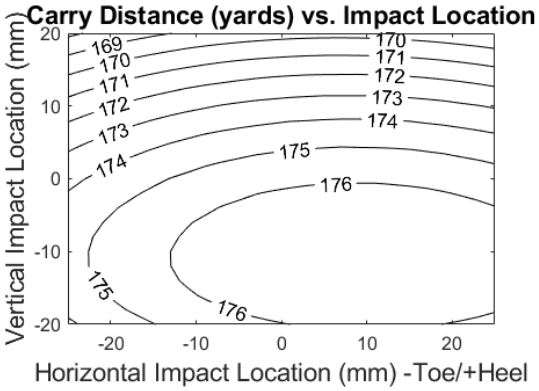

(a) Carry distance without GRFs.

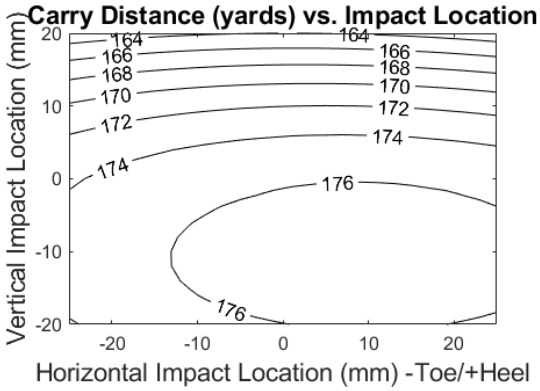

(b) Carry distance with GRFs.

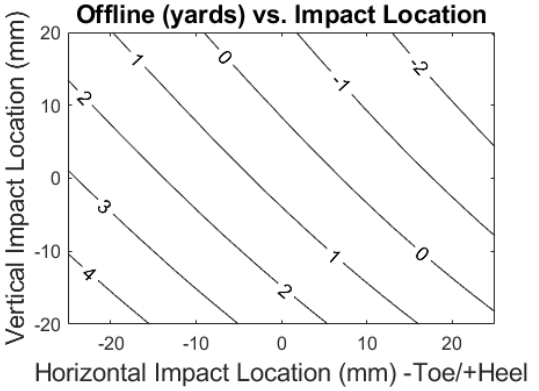

(c) Offline distance without GRFs.

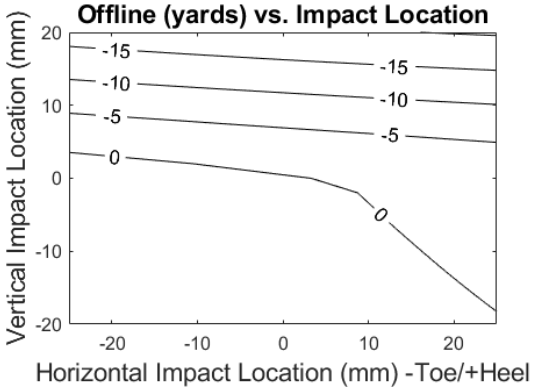

(d) Offline distance with GRFs.

Figure 4.17: Predicted carry distance and offline distance of the 7-iron models.

reaction forces could be measured in a laboratory using force plates. This would require many sod samples from golf courses (the upper layer of grass, roots, and soil). Given that the purpose of this model is to study the effect of fat strikes, the predicted launch conditions of the ball are more important here than comparing the GRFs. In 2021, Corke *et al* published an experimental study to determine the effect of clubhead delivery on launch conditions for an iron shot [56]. The results of this experimental study align well with the results of the new GRF model. Corke *et al* authors found the highest ball speeds occurred for impacts between the centre line of the clubface and 10 mm below. The authors also concluded that the reduction in ball speed for fat strikes is minimal, which is consistent with figure 4.11. Additionally, Most fat strikes saw ball speed decrease by 8 mph or less. In conclusion, the qualitative behavior of this model is consistent with experimental observations. Future experimental studies can be performed to determine more accurate soil parameters.

This new GRF model demonstrates the importance of precise and consistent ball striking. In 2021, PGA tour players averaged 9.2 yards from the hole for approach shots between 150-175 yards [4]. This model predicts fat strikes can land over 12 yards shorter and 15 yards offline. This would more than likely result in missing the green. On the other hand, if the ground reaction forces were not considered, the same shot would be much closer to the target. Therefore, it is important to include ground reaction forces to predict the outcome of iron shots.

Chapter 5

Conclusions

This chapter summarizes the work completed and the findings based on the results. In addition, this chapter discusses some applications for these models and areas for future research.

5.1 Project Summary

The main goal of this work was to develop and compare several impact models to predict the launch conditions of a golf shot. There is a substantial amount of published research for modeling the driver. There are also many publications studying the impact between a golf ball and a rigid surface. There are a few 2D models to predict the launch angle and backspin for iron shots. However, prior to this thesis, there were no 3D models to predict the launch conditions for an iron shot. A significant portion of this work is extending existing impact models for this purpose.

First, the Cross and Dewhurst IM-based model was extended to a 3D impact model. A second horizontal COR term was added to prescribe the amount of slip along the horizontal axis. Additionally, the new model considers the angular velocity of the clubhead. Next, the Maw and Arakawa impact models were extended. A Hunt-Crossly dampening parameter was added in the normal direction to produce inelastic collisions. These contact models were used in a 3D multibody dynamics simulation of the impact between a golf clubhead

and golf ball. This demonstrates that existing 2D impact models can be altered into new 3D models for the collision between two bodies.

These new impact models were elvauted using experimental data. First, the data was used to determine the unique parameters of each model. An optimization approach was used to tune these parameters. The objective function was to minimize the difference between the predicted and measured launch conditions. The conclusions from these results are divided into two groups. First, the results for the driver models are discussed. Then the results for the 7-iron models are considered.

5.1.1 Modeling Driver Impacts

For modeling the driver, the adjusted IM model proposed by Danaei *et al* is the best overall for accuracy. These adjustments improved the accuracy of all launch conditions. The IM model proposed by Cross and Dewhurst were marginally improved compared to the standard IM model. This is reflected in the optimized slip parameters being close to zero. Therefore, assuming a pure rolling condition to model driver impacts is a reasonable assumption.

None of the continuous impact models performed better than the adjusted IM model. The two-layer ball model with the volumetric contact model performed the best of the continuous models. Interestingly, launch angle error is slightly better with the continuous models. Comparing the other error terms reveals they are in the same range compared to IM models. The largest difference is in sidespin error, which is 15% higher for the continuous model. In conclusion, continuous impact models are still a viable option to model driver impacts but need improvements.

5.1.2 Modeling Iron Impacts

For modeling the 7-iron, the two-layer ball with a volumetric normal force model is the best for overall accuracy. The Maw model also performed very well and had the least ball speed error of the models considered. The Arakawa tangential force model had dramatically less accuracy than the others. The IM based 7-iron models demonstrated similar accuracy compared to the IM driver models. The adjusted IM 7-iron model required nearly 4 times the mass added to the clubhead and a greater change in ball CG compared to the driver

models. The Cross and Dewhurst slip model showed the ball spin is greater, by about 4%, than assuming a pure rolling condition. This result suggests that some of the assumptions made by IM models may not be as accurate for modeling higher-lofted clubs. However, these IM models require two orders of magnitude less computing time compared to the continuous models. Therefore, IM-based models can be a useful tool to model 7-iron impacts as well.

When ground reaction forces are applied to the iron model, it can significantly change the behavior of fat strikes. This is when the clubhead makes contact with the ground before the ball. The model shows that ground reaction forces reduced clubhead speed and negatively affected its orientation. This results in the ball travelling less overall distance and substantially offline. To include a ground contact model, the impact model must be continuous. While this model was not directly compared against experimental data, the decrease in ball speed for fat strikes follows similar trends to other experimental studies.

5.2 Recommendations

Based on the results in chapters 3 and 4, the following recommendations are made regarding modeling golf clubhead-ball impacts:

- Existing contact models can be modified to predict inelastic collisions. These new models can be used in dynamic simulations to predict golf impacts.
- Irons and higher lofted clubs benefit more from using continuous impact models compared to drivers. These models consider the deformation of the ball and allow the point of contact to change during impact.
- The behavior of off-centre hits for irons follow the same trends as the driver, but to a lesser degree. Strikes lower on the clubface increase backspin and strikes higher on the clubface reduce backspin. Similarly, strikes towards the toe increase draw spin, while strikes towards the heel increase fade spin. For off-centre driver impacts, this behavior is referred to as the gear effect and it is well documented for drivers.
- Modeling the ground reaction forces has a significant effect for iron shots that impact the ball above the center line of the clubface face. Simulating these shots resulted in a 12% decrease in distance and the ball finishing significantly offline.

5.3 Future Research

Currently there are a few biomechanical golfer models published to predict a drive [30, 60, 61]. The 7-iron model could be combined with one of these predictive golfer models to run simulation experiments. Some potential uses are:

- Investigate the effects of shaft stiffness on biomechanics and ball launch conditions. With the driver models, the focus is usually to maximize clubhead speed. For irons, the launch angle and spin rate are more important as they influence the ball's chance of landing and remaining on a green.
- A set of irons will have different shaft lengths, lofts, and clubhead masses. This is to control the distance of each club. This model could be used to investigate the optimal increments for loft or mass in a set of irons.
- Investigate the effect of vertical MOI (moment of inertia) on golfer biomechanics and accuracy. Essentially, one could compare a larger cavity back iron to a thin blade design.

There are also opportunities for future research to improve the accuracy of the models. The biggest limitation is the data itself. Due to the high clubhead speeds during a swing, it is necessary to extrapolate the data to estimate the kinematics at the exact moment of impact. This is likely a significant portion of the sidespin and horizontal launch angle error. To reduce this error, experiments need to be recorded at higher framerates. With more points, higher-order extrapolation methods could be used. Also, more data points will reduce the extrapolation error. This will provide a better estimate of impact location and face orientation.

Furthermore, additional motion capture experiments should use a wider range of participants. For the driver, there are 550 shots recorded. However, all shots are recorded with elite male players. As a result, the clubhead delivery is very consistent across participants. For example, the mean clubhead speed is 113 mph with a standard deviation under 4 mph. It would be better to validate these impact models with a larger range of abilities. This should produce a richer data set with more variation in club kinematics.

The 7-iron data only consists of 120 shots. The two-layer ball model has 6 model parameters that were identified using this data. When fitting this many variables to a

model, it would be preferred to have more data. Again, having golfers with a larger range of ability and different clubhead speeds is also beneficial. In a set of irons, clubhead mass and loft vary significantly between clubs. Therefore, recording shots with different club properties and validating against this data would be valuable. It would be ideal to have a parameterized model that is validated for a variety of club types.

The ground contact model developed in chapter 4 only considers the soil. This may be adequate for hitting off short grass such as on a tee box or fairway. However, this model is not representative of taller cuts of grass. This model could be modified to capture this behavior without modeling the grass itself. In 2008, the USGA sought to find a surrogate for hitting shots from the rough (taller and thicker area of grass) [37]. This needed to be repeatable and suitable for indoor use. The authors proposed applying wet newsprint or another wet fabric to the ball. This reproduced similar ball flight characteristics to hitting shots from the rough. Therefore, this model may be able to predict shots from the rough by decreasing friction parameters between the ball and clubhead based on conditions.

Lastly, the sole geometry used in chapter 4 (which is modeled as a constant radius) is traditional but still frequently used today. However, in recent years equipment manufacturers have developed several new sole shapes which they claim have certain performance benefits. New models could be constructed for these sole geometries based on the methods in chapter 4. This would give a quantitative comparison of these designs.

References

[1] The Royal & Ancient Golf Club of St Andrews. Record numbers now playing golf worldwide, Dec 2021. Available at: https://www.randa.org/en/articles/record-numbers-now-playing-golf-worldwide, accessed Sep 2022.

[2] Golf Canada. Golfer demographics: How many canadians are golfing?, Dec 2021. Available at: https://canadagolfs.ca/golfer-demographics-canada/, accessed Sep 2022.

[3] E. Matuszewski. The economic impact of golf: $84 billion in the u.s., April 2018. Available at: https://www.forbes.com/sites/erikmatuszewski/2018/04/24/the-economic-impact-of-golf-84-billion-in-the-u-s/?sh=8aa507346eec, accessed Sep 2022.

[4] PGA Stats. Pga tour statistics, 2022. Available at: https://www.pgatour.com/content/pgatour/stats/. Accessed: Aug 2022.

[5] A. Meyers. You won't believe how much farther pga tour champions players are hitting the ball now than in their primes, 2017. Available at: https://www.golfdigest.com/story/you-wont-believe-how-much-farther-pga-tour-champions-players-are-hitting-the-ball-now-than-in-their-primes. Accessed: Spe 2022.

[6] A. Cochran. The impact of science and technology on golf equipment — a personal view. *The Engineering of Sport*, 4:3–15, 2002.

[7] J. McPhee. A review of dynamic models and measurements in golf. *Sports Eng*, 25, 22, 2022.

[8] E. Johnson and M. Stachura. Golf equipment truths: Iron faces are nearly as fast as a driver's. here's why, 2019. Available at: https://www.golfdigest.com/story/golf-equipment-truths-iron-faces-are-nearly-as-fast-as-a-drivers-heres-why. Accessed: Nov 2022 Nov 2022.

[9] A. Bejan, S. Lorente, J. Royce, D. Faurie, T. Parran, M. Black, and B. Ash. The constructal evolution of sports with throwing motion: Baseball, golf, hockey and boxing. *International Journal of Design and Nature and Ecodynamics*, 8(1), 2013. ISSN 17557437. doi: 10.2495/DNE-V8-N1-1-16.

[10] The R&A and USGA. The equipment rules, 2019. Available at: https://www.usga.org/content/dam/usga/pdf/Equipment/Equipment20Rules20Final.pdf Accessed: Oct. 2022.

[11] A.J. Cochran and J.Stobbs. *The search for the perfect swing*. Morrison & Gibb Ltd, London, 1968.

[12] J. R. Roberts, R. Jones, and S. J. Rothberg. Measurement of contact time in short duration sports ball impacts: an experimental method and correlation with the perceptions of elite golfers. *Sports Engineering*, 4(4), 2001. ISSN 1369-7072. doi: 10.1046/j.1460-2687.2001.00084.x.

[13] K. Arakawa, T. Mada, H. Komatsu, T. Shimizu, M. Satou, K. Takehara, and G. Etoh. Dynamic deformation behavior of a golf ball during normal impact. *Experimental Mechanics*, 49(4), 2009. ISSN 00144851. doi: 10.1007/s11340-008-9156-y.

[14] W. Petersen and J. McPhee. Comparison of impulse-momentum and finite element models for impact between golf ball and clubhead. In *World Scientific Congress of Golf V*, Phoenix, 2008.

[15] A. R. Penner. The physics of golf: The convex face of a driver. *American Journal of Physics*, 69(10), 2001. ISSN 0002-9505. doi: 10.1119/1.1380380.

[16] D. C. Winfield and T. E. Tan. Optimization of clubhead loft and swing elevation angles for maximum distance of a golf drive. *Computers and Structures*, 53(1), 1994. ISSN 00457949. doi: 10.1016/0045-7949(94)90125-2.

[17] D. C. Winfield and Teong E. Tan. Optimization of the clubface shape of a golf driver to minimize dispersion of off-center shots. *Computers and Structures*, 58(6), 1996. ISSN 00457949. doi: 10.1016/0045-7949(95)00220-0.

[18] A. R. Penner. The physics of golf: The optimum loft of a driver. *American Journal of Physics*, 69(5), 2001. ISSN 0002-9505. doi: 10.1119/1.1344164.

[19] P. Chou, D. Liang, J. Yang, and W. Gobush. Contact forces, coefficient of restitution, and spin rate of golf ball impact. In *Science and Golf II*. E & FN Spon, 2021. doi: 10.4324/9780203474709-51.

[20] R. Cross. Grip-slip behavior of a bouncing ball. *American Journal of Physics*, 70(11), 2002. ISSN 0002-9505. doi: 10.1119/1.1507792.

[21] R. Cross and P. Dewhurst. Launch speed, angle and spin in golf. *European Journal of Physics*, 39(6), 2018. ISSN 13616404. doi: 10.1088/1361-6404/aadda8.

[22] F. Berkshire. The science of the perfect swing, by P. Dewhurst. *Contemporary Physics*, 58(4), 2017. ISSN 0010-7514. doi: 10.1080/00107514.2017.1344319.

[23] B. Danaei, W. McNally, E. Henrikson, and J. McPhee. Adjusting a Momentum-Based Golf Clubhead-Ball Impact Model to Improve Accuracy. *Proceedings*, 49(1), 2020. ISSN 2504-3900. doi: 10.3390/proceedings2020049047.

[24] N. M. Lindsay. Topspin in putters — a study of vertical gear-effect and its dependence on shaft coupling. *Sports Engineering*, 6(2), 2003. ISSN 1369-7072. doi: 10.1007/bf02903530.

[25] J Lambeth, D. Brekke, and J. Brunski. Exploration of center of gravity, moment of inertia, and launch direction for putters with ball speed normalizing face properties. In *The 13th Conference of the International Sports Engineering Association*, 2020. doi: 10.3390/proceedings2020049002.

[26] K. H. Hunt and F. R.E. Crossley. Coefficient of restitution interpreted as damping in vibroimpact. *Journal of Applied Mechanics, Transactions ASME*, 42(2), 1975. ISSN 15289036. doi: 10.1115/1.3423596.

[27] B. Lieberman and S. Johnson. An analytical model for ball-barrier impact: Part 1: Models for normal impact. In *Science and Golf II*. 2021. doi: 10.4324/9780203474709-53.

[28] A. J. Cochran. Development and use of one-dimensional models of a golf ball. In *Journal of Sports Sciences*, volume 20, 2002. doi: 10.1080/026404102320183202.

[29] Y. Gonthier, J. McPhee, and C. Lange. On the implementation of coulomb friction in a volumetric-based model for contact dynamics. In *2007 Proceedings of the ASME International Design Engineering Technical Conferences and Computers and Information in Engineering Conference, DETC2007*, volume 5 PART A, 2008. doi: 10.1115/DETC2007-35311.

[30] W. McNally and J. McPhee. Dynamic Optimization of the Golf Swing Using a Six Degree-of-Freedom Biomechanical Model. In *Proceedings*, 2018. doi: 10.3390/proceedings2060243.

[31] M. Nakasuga and R. Hashimoto. Measurement of tangential force of golf ball impact. *Proceedings of the Japan Society of Mechanical Engineers*, pages 97–102, 1997.

[32] E. Henrikson, P. Wood, C. Broadie, and T. Nuttall. The Role of Friction and Tangential Compliance on the Resultant Launch Angle of a Golf Ball. In *Proceedings*, 2020. doi: 10.3390/proceedings2020049027.

[33] T. Iwatsubo, S. Kawamura, K. Miyamoto, and T. Yamaguchi. Numerical analysis of golf club head and ball at various impact points. *Sports Engineering*, 3(4), 2000. ISSN 1369-7072. doi: 10.1046/j.1460-2687.2000.00055.x.

[34] K. Tanaka, H. Oodaira, S. Ujihashi, F. Sato, Y. Teranishi, and F. Sato. Construction of the Finite-Element Models of Golf Balls and Simulations of Their Collisions. *Proceedings of the Institution of Mechanical Engineers, Part L: Journal of Materials Design and Applications*, 220(1), 2006. ISSN 20413076. doi: 10.1243/14644207JMDA80.

[35] N. Maw, J. R. Barber, and J. N. Fawcett. The oblique impact of elastic spheres. *Wear*, 38(1), 1976. ISSN 00431648. doi: 10.1016/0043-1648(76)90201-5.

[36] W. J. Stronge, R. James, and B. Ravani. Oblique impact with friction and tangential compliance. *Philosophical Transactions of the Royal Society A: Mathematical, Physical and Engineering Sciences*, 359(1789), 2001. ISSN 1364503X. doi: 10.1098/rsta.2001.0903.

[37] USGA and R&A. Interim report: study of spin generation, 2006.

[38] P. Brown and J. McPhee. A Continuous Velocity-Based Friction Model for Dynamics and Control with Physically Meaningful Parameters. *Journal of Computational and Nonlinear Dynamics*, 11(5), 2016. ISSN 15551423. doi: 10.1115/1.4033658.

[39] Z. Q. Wu, Y. Sogabe, Y. Arimitsu, and T. Tamaogi. Design of golf club and ball with numerical experiment. In *Proceedings of the SEM Annual Conference and Exposition on Experimental and Applied Mechanics 2007*, volume 2, 2007.

[40] K. Tanaka, H. Oodaira, Y. Teranishi, F. Sato, and S. Ujihashi. Finite-Element Analysis of the Collision and Bounce between a Golf Ball and Simplified Clubs (P271). In *The Engineering of Sport 7*. 2009. doi: 10.1007/978-2-287-99056-4{_}78.

[41] W. McNally, J. McPhee, and E. Henrikson. The Golf Shaft's Influence on Clubhead-Ball Impact Dynamics. *Proceedings*, 2(6), 2018. ISSN 2504-3900. doi: 10.3390/proceedings2060245.

[42] S. Kammerer. Golf course fairways - managing quality and playability, 2019. Available at: https://www.usga.org/content/usga/home-page/course-care/green-section-record/57/17/golf-course-fairways–managing-quality-and-playability.html Accessed: Nov. 2022.

[43] J. Sens. 6 grass types every golfer should know, and how each affects your game, 2022. Available at: https://golf.com/lifestyle/grass-types-every-golfer-should-know/ Accessed: Nov. 2022.

[44] S. Kammerer. A rough feature, 2018. Available at: https://www.usga.org/content/usga/home-page/course-care/green-section-record/57/17/golf-course-fairways–managing-quality-and-playability.html Accessed: Nov. 2022.

[45] T. Green. A combination of lightweight rolling and sand topdressing to decrease fungicide inputs and enhance golf course fairway turf. Master's thesis, Michigan State University, 2015.

[46] B. Whitlark. Can sand topdressing make fairways softer?, 2022. Available at: https://www.usga.org/content/usga/home-page/course-care/green-section-record/60/18/can-sand-topdressing-make-fairways-softer-.html Accessed: Nov. 2022.

[47] S. J. Hakke. *Apparatus and test methods for measuring the impact of golf balls on turf and their application in the field*. PhD thesis, Aston University, UK, 1990.

[48] A. R. Penner. The run of a golf ball. *Canadian Journal of Physics*, 80(8), 2002. ISSN 00084204. doi: 10.1139/p02-035.

[49] USGA and R&A. Proposed bounce model for use in evaluating optimum overall distance, 2021.

[50] J. Y. Wong. *Terramechanics and Off-Road Vehicle Engineering*. Elsevier, 2010. doi: 10.1016/C2009-0-00403-6.

[51] R. He, C. Sandu, A. K. Khan, A. G. Guthrie, Schalk E., and H. A. Hamersma. Review of terramechanics models and their applicability to real-time applications. *Journal of Terramechanics*, 81, 2019. ISSN 00224898. doi: 10.1016/j.jterra.2018.04.003.

[52] A. Rula, J. Nuttall, and J. Clifford. An analysis of ground mobility models (anamob), 1970. Available at: https://apps.dtic.mil/sti/citations/AD0886513. Accessed: Nov 2022.

[53] J. Wong and A. R. Reece. Soil Failure Beneath Rigid Wheels. In *Proceedings of the Second International Conference on the International Society for Terrain-Vehicle Systems*. 2019. doi: 10.3138/9781487584757-036.

[54] M. Boos and J. McPhee. Volumetric modeling and experimental validation of normal contact dynamic forces. *Journal of Computational and Nonlinear Dynamics*, 8(2), 2013. ISSN 15551415. doi: 10.1115/1.4006836.

[55] R. L. Jackson, H. Ghaednia, H. Lee, A. Rostami, and X. Wang. Contact mechanics. In *Tribology for Scientists and Engineers: From Basics to Advanced Concepts*, volume 9781461419457. 2013. doi: 10.1007/978-1-4614-1945-7{_}3.

[56] T. Corke, N. Betzler, S. Wallace, and S. Otto. Predicting golf ball launch characteristics using iron clubhead presentation variables and the influence of mishits. *Proceedings of the Institution of Mechanical Engineers, Part P: Journal of Sports Engineering and Technology*, 236(2), 2022. ISSN 1754338X. doi: 10.1177/1754337120987857.

[57] M.G. Bekker. *Theory of Land Locomotion*. University of Michigan Press, 2017. doi: 10.3998/mpub.9690401.

[58] M. Bekker. *Introduction to terrian-vehicle systems*. Michigan: The University of Michigan Press, Ann Arbor, 1969.

[59] S. Ferguson, W. McNally, and J. McPhee. Predicting the flight of a golf ball: Comparing a physics-based aerodynamcis model to a neural network. *The Engineering of Sport*, 14, 2022.

[60] I. Kenny, A. McCloy, E. Wallace, and S. Otto. Segmental sequencing of kinetic energy in a computer-simulated golf swing. *Sports Engineering*, 11(1), 2008. ISSN 1369-7072. doi: 10.1007/s12283-008-0005-0.

[61] C. Brown, W. McNally, and J. McPhee. Optimal control of joint torques using direct collocation to maximize ball carry distance in a golf swing. *Multibody System Dynamics*, 50(3), 2020. ISSN 1573272X. doi: 10.1007/s11044-020-09734-0.

[62] P. C. Chou, D. Liang, J. Yang, and W. Gobush. Contact forces, coefficient of restitution, and spin rate of golf ball impact. In *Science and Golf II*. 2021. doi: 10.4324/9780203474709-51.

[63] W. McNally and J. McPhee. Investigating the Influence of Shaft Balance Point on Clubhead Speed: A Simulation Study. In *Proceedings*, 2020. doi: 10.3390/proceedings2020049156.

[64] E. Henrikson, P. Wood, C. Broadie, and T. Nuttall. The Role of Friction and Tangential Compliance on the Resultant Launch Angle of a Golf Ball. In *Proceedings*, 2020. doi: 10.3390/proceedings2020049027.